Wireless And Passive Multi-Sensor Platform Using A Single Antenna

by

Muhammad Junaid Akhtar

A Dissertation Submitted to the
Graduate School of Sciences and Engineering
in Partial Fulfillment of the Requirements for
the Degree of

Master of Science

in

Electrical and Electronics Engineering

KOÇ ÜNİVERSİTESİ

October, 2022

Wireless And Passive Multi-Sensor Platform Using A Single Antenna

Koç University
Graduate School of Sciences and Engineering
This is to certify that I have examined this copy of a master's thesis by

Muhammad Junaid Akhtar

and have found that it is complete and satisfactory in all respects, and
that any and all revisions required by the final
examining committee have been made.

Committee Members:

Asst. Prof. Dr. Levent Beker (Advisor)

Asst. Prof. Dr. Muhammad Ilyas

Asst. Prof. Dr. Murat Kuşcu

Date:

To my parents, wife, and kids!

ABSTRACT

Wireless And Passive Multi-Sensor Platform Using A Single Antenna
Muhammad Junaid Akhtar
Master of Science in Electrical and Electronics Engineering
October, 2022

Near field resonant inductive coupling (NRIC) is one of the oldest and predominant wireless communication methods with an implanted medical device (IMD). In this approach, an inductor coupled with a sensor makes an LC resonator. Any change in the sensor's output is reflected as a change in its capacitance, which in turn leads to a shift in this LC resonator's resonance frequency. Shift in this resonance frequency can be tracked wirelessly by measuring the output impedance/reflection coefficient of an external reader antenna in the near field of the implanted device. In most current devices, data from multiple sensors is required simultaneously. In this work, we propose a simple configuration to simultaneously sense various parameters from one antenna. By tapping the inductor at different locations, we get two sub-inductors. We connect two capacitive sensors with the sub-inductors to get two LC loops. The scope of this thesis is the design of such an antenna through simulations, its fabrication, and characterization with two sensors simultaneously to demonstrate its feasibility in potential IMD applications.

Key Words: Near field inductive coupling, LC resonator, resonance frequency

ÖZETÇE

Tek Anten Kullanan Kablosuz ve Pasif Çoklu Sensör Platformu

Muhammad Junaid Akhtar

Elektrik ve Elektronik Mühendisliği, Yüksek Lisans

Ekim, 2022

Yakın alan rezonans endüktif kuplaj (NRIC), implante tıbbi cihaz (IMD) ile en eski ve baskın kablosuz iletişim yöntemlerinden biridir. Bu yaklaşımda, bir sensörle birleştirilmiş bir indüktör, bir LC rezonatörü oluşturur. Sensörün çıkışındaki herhangi bir değişiklik, kapasitansında bir değişiklik olarak yansıtılır ve bu da bu LC rezonatörünün rezonans frekansında bir kaymaya yol açar. Bu rezonans frekansındaki kayma, implante edilen cihazın yakın alanındaki bir harici okuyucu antenin çıkış empedansı/yansıma katsayısı ölçülerek kablosuz olarak izlenebilir. Mevcut cihazların çoğunda, aynı anda birden fazla sensörden gelen veriler gereklidir. Bu çalışmada, bir antenden çeşitli parametreleri aynı anda algılamak için basit bir konfigürasyon öneriyoruz. İndüktöre farklı yerlere dokunarak iki alt indüktör elde ederiz. İki LC döngüsü elde etmek için iki kapasitif sensörü alt indüktörlere bağlarız. Bu tezin kapsamı, potansiyel IMD uygulamalarında uygulanabilirliğini göstermek için simülasyonlar yoluyla böyle bir antenin tasarımı, üretimi ve aynı anda iki sensörle karakterizasyonudur.

Anahtar Kelimeler: Yakın alan endüktif kuplaj, LC rezonatör, rezonans frekansı

ACKNOWLEDGMENTS

I am very thankful to Dr. Levent Beker for giving me an opportunity to work on multi-parameter sensing antenna and for his guidance and support during my research work. I am thankful to all my colleagues in Bio-integrated Microdevices Lab (BMDL). I am very thankful to Fariborz Mirlou, Azmatullah, and Awais for their support during fabrication and soldering processes. I am also thankful to Javad for his support in the design of interdigitated capacitive strain sensors (ICSS). I am also very grateful for my friends and family, especially my wife and parents.

TABLE OF CONTENTS

LIST OF TABLES

LIST OF FIGURES

ABBREVIATIONS

NRIC	Near-field resonant inductive coupling
IMD	Implantable Medical Device
ICSS	Interdigitated Capacitive Strain Sensors
VNA	Vector Network Analyzer

Chapter 1

INTRODUCTION

1.1 Wireless passive sensing

Implantable medical devices (IMDs) are widely used in health-monitoring systems, where they keep track of data without human interference. IMDs are used for the measurement and monitoring of multiple body parameters. IMDs help prevent and handle chronic health conditions and improve the quality of life. Obtaining sensor data from an IMD is a critical design step [Dey et al., 2019]. In wired sensors, the sensor and reader side communicate through cables. These transcutaneous wires can increase the risk of infection and restrict patient mobility, significantly deteriorating the patients' safety and well-being. Passive operation, where there is no power side on the sensor side, is also desirable. Therefore, wireless and passive operation is suitable for obtaining data from implanted biomedical sensors. Many industrial and automotive applications also require sensing of physical or chemical quantities in harsh environments [Li *et al.*, 2015], where a wired connection to the sensor cannot be established. Examples of these systems include non-contact structural monitoring of concrete structures, tire-pressure monitoring, and high-temperature measurement [Nopper *et al.*, 2010] [Babu and George, 2016]. Therefore, wireless passive sensing is the preferred method to obtain sensor data in harsh environments, where measurement by direct physical contact is problematic. Some current techniques to receive sensor data are ultrasound and near-field resonant inductive coupling (NRIC) [Karimi *et al.*, 2021].

In an ultrasonic-based sensor node, we have an ultrasonic communication device such as a piezo resonator attached to a sensor. The piezo resonator functions as an acoustic antenna, which enables the sensor to receive ultrasonic waves from an external transducer. Changes in the sensor's measured parameter alter the piezo's acoustic reflection coefficient, leading to backscattered signal's (echo) amplitude modulation. The piezo then transmits this modulated signal back to the external transducer, where the signal is processed to extract the data (i.e., sensor response) [Akhtar, 2021]. A drawback of ultrasound is that it cannot penetrate across the skull because bones attenuate the ultrasound signals through them very highly [Bhar and Mandal, 2022].

NRIC is the oldest and predominant wireless communication method with an IMD or remote sensor. Less complex hardware, continuous monitoring capability, and operation at lower operating frequencies are advantages of NRIC compared to other wireless systems [Babu and George, 2016]. A typical scenario is shown in Figure 1.1. There are two systems in this mechanism. One is called the sensing circuit, and the second system is called the reader circuit, which is separate from the sensing circuit. It is only used when data is to be measured from the sensor. The reader circuit consists of a reader coil with a high frequency sweeping device, such as a vector network analyzer (VNA) or impedance analyzer. The sensing circuit includes a secondary coil attached to a sensor. The sensor's output is reflected as some capacitance value, making the sensing circuit an LC resonator with a particular resonance frequency. Any change in the parameter being measured alters the capacitance of this LC resonator, thereby changing its resonance frequency. This resonance frequency can be tracked wirelessly by observing the reader circuit's output impedance/reflection coefficient by placing the reader coil in the near field of the sensing circuit / implanted device. The passive wireless properties make LC resonator-based sensors highly suitable for IMDs, wearables, and in applications where getting physical access to the sensor chip is difficult, such as in sealed or harsh environments.

1.2 The system model of LC resonator-based sensors

To understand the working principle of LC sensors, their circuit equivalent representation is shown in Figure 1.2. The reading coil represents an equivalent series resistance R_p and inductance L_p. R_s and L_s denote the sensing coil's equivalent series resistance and inductance, respectively. The sensor is represented by a variable capacitance C_s [Lin *et al.*, 2021]. The two coils have a mutual inductance M between them. I_p and I_s are the currents through reading and sensing coils, respectively. The reader coil and sensing circuit present an equivalent impedance (Z_{in}) to the VNA due to mutual coupling [Huang *et al.*, 2016].

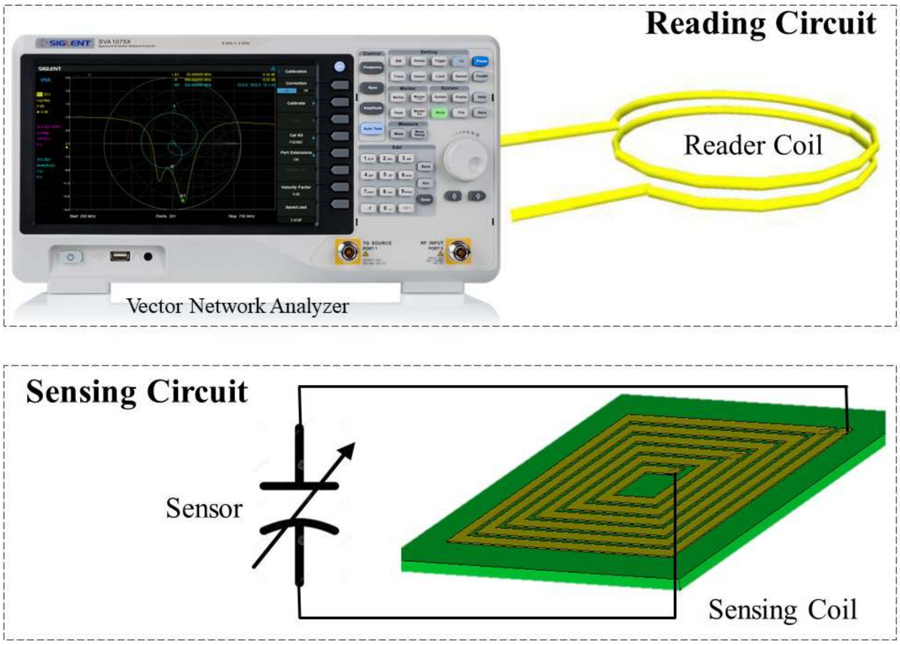

Figure 1.1: A typical LC passive measurement system.

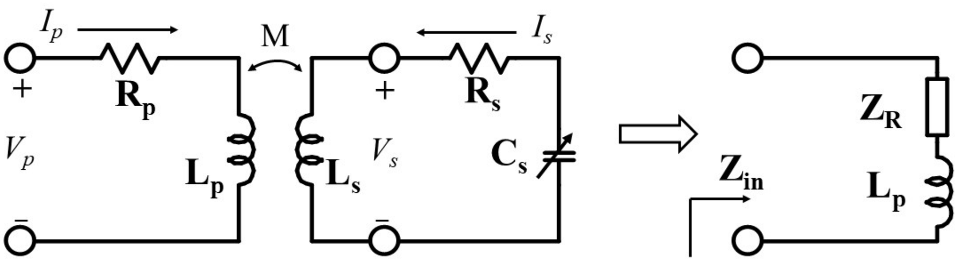

Figure 1.2: Equivalent circuit representation of LC-based sensor.

Using Kirchhoff's voltage law, we can write:

$$V_p = R_p I_p + j\omega L_p I_p + j\omega M I_s \tag{1.1}$$

$$V_s = j\omega L_s I_s + j\omega M I_p = -R_s I_s - \frac{I_s}{j\omega C_s} \tag{1.2}$$

M represents the mutual inductance between two coils, and it is given by:

$$M = k\sqrt{L_p L_s} \tag{1.3}$$

where *k* is the coupling coefficient between the two inductors [Zhou *et al.*, 2021]. The value of *k* depends upon the geometry, distance, and relative angle between the coils [Degen, 2021]. No coupling between the coils means k=0, and maximum coupling implies k=1. From a measurement point of view, the positions of the reader and sensor coils should be fixed to get a constant *k*. The equivalent input impedance seen by the VNA at the reader coil can be derived using equations 1.1 and 1.2:

$$Z_{in} = \frac{V_p}{I_p} = Z_R + j\omega L_p = j\omega L_p + R_p + \frac{\omega^2 M^2}{R_s + j\omega L_s + 1/j\omega C_s} \tag{1.4}$$

Now we define the resonance frequency and Q-factor of the LC sensor as:

$$f_r = \frac{1}{2\pi\sqrt{L_s C_s}} \tag{1.5}$$

$$Q = \frac{1}{R_s}\sqrt{\frac{L_s}{C_s}} \tag{1.6}$$

After putting the values of *M*, f_s, and *Q* in equation 1.4, the input impedance can then be re-written as:

$$Z_{in} = R_p + j\omega L_p + \left(1 + \frac{k^2\left(\frac{f}{f_r}\right)^2}{1 + j\frac{1}{Q}\frac{f}{f_r} - \left(\frac{f}{f_r}\right)^2}\right) \tag{1.7}$$

The input impedance can be decomposed into real and imaginary parts as follows:

$$\mathrm{Re}\{Z_{in}\}=R_p+\omega L_p k^2 Q \frac{\frac{f}{f_r}}{1+Q^2\left(\frac{f}{f_r}-\frac{f_r}{f}\right)^2} \tag{1.8}$$

$$\mathrm{Im}\{Z_{in}\}=\omega L_p\left(1+k^2Q^2\frac{1-\left(\frac{f}{f_r}\right)^2}{1+Q^2\left(\frac{f}{f_r}-\frac{f_r}{f}\right)^2}\right) \tag{1.9}$$

At the resonance frequency $f=f_r$, and by using equation 1.8, we see that the real part of input impedance will be at its maximum value at the resonance frequency. This value is given by:

$$Z_{max}=\mathrm{Re}\{Z_{in}\}=R_p+\omega L_p k^2 Q \tag{1.10}$$

Therefore, if we observe the real part of the input impedance of the reader coil, we will observe a peak at the resonance frequency. Practically, to measure the resonant frequency, we measure the S11 parameter on a Vector Network Analyzer (VNA). There is a sharp dip in S11 magnitude vs. frequency at the resonance frequency. S11 measures the degree of matching between the characteristic impedance of the vector network analyzer (typically Z_0=50Ω) and the impedance of the load (Z_{in}).

$$S11=20\log_{10}(|\Gamma|) \tag{1.11}$$

Where Γ is the reflection coefficient. It is the ratio of the amplitude of the reflected wave to the incident wave. It is determined by the load/device impedance and the internal impedance of the VNA. It is defined mathematically as:

$$\Gamma=\frac{Z_{in}-Z_0}{Z_{in}+Z_0} \tag{1.12}$$

After finding the resonance frequency f_r, we can find the sensor capacitance C_s by putting f_r it into equation 1.5, along with already known inductance L_s of the sensor coil.

1.3 Multiple parameter sensing

Typically, LC sensors can only be used to detect a single parameter because an inductor coupled with a capacitor has only one resonance frequency. If two or more capacitive sensors are connected to the inductor simultaneously, they will lead to an equivalent capacitance depending upon whether they are connected in series or parallel. This new capacitance will again have a single resonance frequency, which will change with variation in capacitance of any one of the sensors. Therefore, distinguishing multiple sensor outputs from this single resonance frequency is not possible. Demand for IMDs which can sense multiple biological parameters simultaneously has increased rapidly. Apart from IMDs, devices in the industry are also being developed that measure multiple parameters from remote sensors. Multi-parameter sensors can save space and reduce measurement costs. Several strategies have been employed to measure multiple parameters using LC sensors simultaneously.

1.3.1. Resonance frequency and Q-factor

The most common approach to obtain data from two sensors is using resonant frequency (frequency of minima in S11 curve) and Q-factor (amplitude of S11 curve at resonance). This method was applied for simultaneous temperature and pressure measurements in [Zhang *et al.*, 2019]. The sensor was designed such that the temperature changes the resistivity of the sensor, and pressure changes its capacitance. A change in capacitance changes the resonant frequency. So, the temperature is measured by following the resonance frequency. Resistivity varies the amplitude of S11 at the resonant frequency. So, pressure is measured by tracking the amplitude of S11 at resonance. A remote, temperature compensated pH sensor for wireless and passive temperature/pH sensing was presented in [Bhadra *et al.*, 2013]. A temperature-dependent resistor was used to detect the pH variation by a shift in the resonant frequency, and the Q factor was used to detect the temperature. A sensor measuring the conductivity and dielectric constant was presented in [Zhang *et al.*, 2012]. The phase dip amplitude is changed by both conductivity and dielectric constant, while a change in dielectric constant is reflected as a resonant frequency shift. This approach can be problematic because resonance frequency change is often accompanied by amplitude change by default, which makes accurate sensing of the second sensor difficult. The approach in [Bhadra *et al.*, 2013; Zhang *et al.*, 2019], [Zhang *et al.*, 2012] is only suitable when one of the parameters to be measured depends upon the same sensors' resistance. This method cannot be used when both the sensors are capacitive in nature.

1.3.2. Using multiple inductors

Multiple parameters can also be measured by using multiple inductors and coupling each of them with sensors in an array. This can lead to a large sensing circuit size, requiring a large reader antenna. To decrease the area, different configurations have been proposed. The sensor area can be decreased by stacking the inductors. A drawback of this stacking up is strong mutual coupling between the inductors. To minimize the mutual coupling, a configuration was proposed in [Dong *et al.*, 2015] by coaxially putting the second layer inductor above the first layer inductor, and a specific winding is used to minimize mutual inductance between them. In this winding, the rotation direction of adjacent loops is opposite, and there must be an even number of turns. A branching inductor is proposed in [Dong *et al.*, 2019]. The branches are distributed on the front and bottom layers of the substrate. Each front layer branch has its counterpart on the bottom layer. By folding the structure along its symmetry axis, it is shaped as a double-layer inductor with different sub-inductors. Capacitive sensors are connected with these sub-inductors resulting in multiple resonance frequencies. A configuration of multiple partially overlapped LC sensors is proposed in [Sancho *et al.*, 2019]. The mutual inductance is minimized by using partially overlapped coils or decoupling coils. All these methods use multiple inductors to achieve multi-parameter measurement.

1.3.3. Single inductor with active elements

By incorporating active elements in the design, dual resonance can be achieved [Barakat *et al.*, 2019] [Deng et al., 2019]. A configuration using a single inductor to measure multiple parameters was proposed in [Dong et al., 2016]. Here, two sensors were coupled to a single inductor through a relay switch in time-division multiplexing. When the switch is turned on, one capacitive sensor is connected to the inductor, while the second sensor is disconnected. When the switch is off, the second sensor is connected to the inductor, and the first one is disconnected. So, at one time, only one capacitor is connected to the inductor making an LC sensor with a particular resonant frequency. This approach was used to measure pressure and humidity. However, this method does not measure both parameters simultaneously, and adding the rectifier and switch takes extra space, which increases the area of the sensor.

1.4 This work – Multiparameter sensing with single inductor

This thesis presents a scheme for simultaneous wireless passive sensing of multiple parameters using a single planar inductor without any switching elements. In this approach, two capacitive sensors are connected to the same inductor at different turn locations. In this way, one inductor is divided into two sub-inductors. Depending upon the turns where these sensors are connected, each sub-inductor has a particular inductance value different from the other. A schematic of the concept is shown in Figure 1.3. Like Figure 1.1, L_p and R_p represent the inductance and equivalent resistance of the primary or reader loop. The inductance of the two sub-inductors is represented by L_1 and L_2, respectively. R_1 and R_2 represent their respective equivalent series resistances.

When two separate sensors with capacitance C_1 and C_2 are connected to the sub-inductors L_1 and L_2, they make two resonant LC circuits. Both LC circuits have different resonance frequencies that can be used to track the value of the respective sensor separately. The reader loop is connected to a VNA, which measures its S11. Dips in the S11 plot vs. frequency show the resonance frequencies of the LC circuits. The resonance frequencies are given by:

$$f_1 = \frac{1}{2\pi\sqrt{L_1 C_1}} \tag{1.13}$$

$$f_2 = \frac{1}{2\pi\sqrt{L_2 C_2}} \tag{1.14}$$

The loop can be designed to make the inductance values L_1 and L_2 such that the resonance frequencies f_1 and f_2 have sufficient separation. The inductances L_1 and L_2 can be measured with an impedance analyzer, and the frequencies f_1 and f_2 using a vector network analyzer. Knowing these quantities, the value of C_1 and C_2 can be calculated as:

$$C_1 = \frac{1}{4\pi^2 f_1^{\ 2} L_1} \tag{1.15}$$

$$C_2 = \frac{1}{4\pi^2 f_2^{\ 2} L_2} \tag{1.16}$$

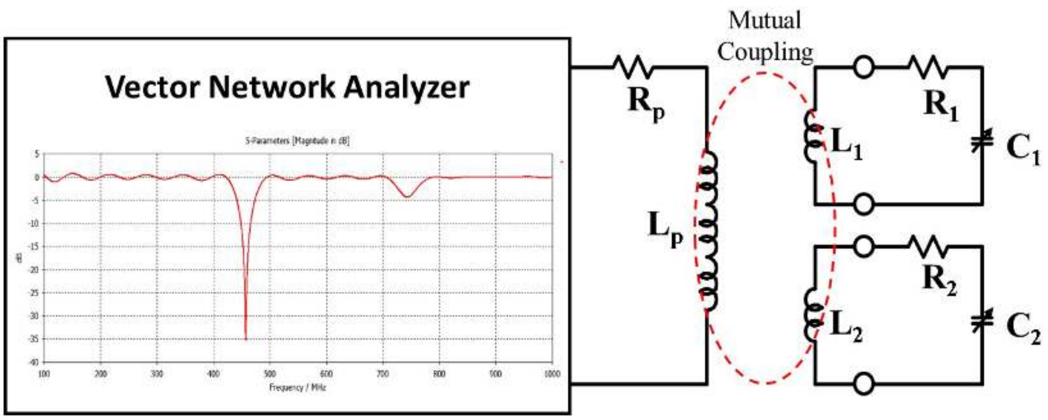

Figure 1.3: Concept of LC passive sensing using a single inductor.

When the output of the sensor is changed, the resonance frequencies f_1 and f_2 change. The new capacitance values can be found by putting these new resonance frequency values in the above equations. Then the actual measured parameter (e.g., strain, pressure, etc.) can be estimated from these capacitance values.

1.5 Thesis outline

In chapter 2, we will cover the design of the inductor on the FR-4 substrate in detail. This will include design, simulations, fabrication, characterization of the inductor, and its comparison with measurements. In chapter 3, the design, simulations, fabrication, and measurement of the inductor with two variable capacitors will be covered. Inductor with two strain sensors on a flexible substrate will be discussed in chapter 4. The thesis will end with a conclusion section in chapter 5.

Chapter 2

PLANAR INDUCTOR

2.1 Basics

An inductor is a passive component that stores energy in a magnetic field when electric current flows through it [Alexander *et al.*, 2006]. Basically, when we wound an insulated wire into a coil, we get an inductor. According to Faraday's law of induction, a magnetic field is generated by a time-varying current, inducing voltage in the conductors. A planar inductor is the one made by etching the conductor onto a printed circuit board in a spiral pattern. A measure of an inductor's magnetic field storage capacity is termed its self-inductance. It is the ratio of induced voltage to the rate of current change. It is measured in Henry (H). 1 henry equals 1 weber/ampere or 1 volt.sec/ampere. When an inductor is placed adjacent to another inductor, the magnetic fields of one inductor induce a voltage in the second inductor. This is called mutual induction or mutual coupling. Recalling equation 1.3, $M=k\sqrt{L_pL_s}$, we see that apart from the position/orientation dependent coupling coefficient *k*, the mutual coupling is also dependent upon the self-inductances of the two coils. Therefore, for better energy/information transfer, we should have inductors with a high inductance value.

2.2 Inductance and geometry

The inductance of a solenoid is directly proportional to the number of turns and its area [Bolz, 1970]. Most sensors are now compact. Also, the area of IMDs has to be kept at a minimum. To increase the self-inductance of a coil in a limited area, we can only increase the number of turns. If the turns are kept constant, we must modify the shape of the spiral pattern so that inductance is maximized. The effects of spiral shape on inductance have been studied in [Luo and Wei, 2018] and [Stojanovic and Zivanov, 2004]. To calculate the DC inductance of spiral inductors of different shapes, simple and accurate expressions were presented by Mohan et al. [Mohan *et al.*, 1999]. Three approximations have been derived and their accuracy evaluated by simulations and measurements. The first approximation is based by modifying the inductance expression developed by Wheeler [Wheeler, 1928]. The second approximation considers the sides of the inductor as current sheets. The third expression is obtained by monomial fitting from measured inductance values from a collection of many inductors. In all the approximations, the thickness of the inductor is ignored because it has a negligible effect on the self-inductance of an inductor. The expressions for calculating inductance are based on geometrical parameters, as defined in Figure 2.1.

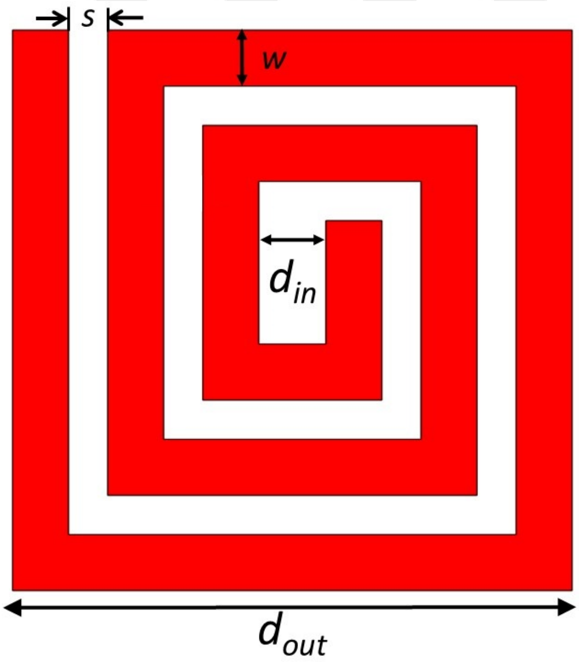

Figure 2.1: Design parameters of a square spiral inductor.

Here N is the number of turns, w is track width, s is spacing between turns, d_{out} is the outer diameter, and d_{in} is the inner diameter. Other parameters that are used in the inductance expressions are average $d_{avg}=(d_{out}+d_{in})/2$ and fill ratio $\rho=(d_{out}-d_{in})/(d_{out}+d_{in})$. The modified formula for inductance based on Wheeler's formula is:

$$L=K_1\mu_0\frac{N^2 d_{avg}}{1+K_2\rho} \tag{2.1}$$

Here μ_0 is the permeability of free space having a value of approximately 12.57×10^{-7} H/m. K_1 and K_2 depend upon the shape of the spiral pattern. For three different shapes, these factors are shown in Table 2.1. The fill ratio becomes vital in determining the inductance for two different inductors with the same average diameter. A small value of ρ means that the inside is hollow towards the center, so the contribution from the inner turns towards mutual inductance is less, which leads to a lower self-inductance value. A high value of ρ means the inner turns will contribute more, and that inductor will have a larger self-inductance.

Table 2.1: Value of K_1 and K_2 for different spiral shapes.

Shape	K_1	K_2
Square	2.34	2.75
Hexagonal	2.33	3.82
Octagonal	2.25	3.55

The current-sheet approximation based expression is as follows:

$$L=\frac{\mu N^2 d_{avg} c_1}{2}\left(\ln(c_2/\rho)+c_3\rho+c_4\rho^2\right) \tag{2.2}$$

The coefficients c_1, c_2, c_3, c_4 are also shape-dependent. Their values for different shapes are shown in Table 2.2. The expression for inductance based on monomial fit is given as:

$$L=\beta d_{out}^{\alpha_1} w^{\alpha_1} d_{avg}^{\alpha_3} N^{\alpha_4} s^{\alpha_5} \tag{2.3}$$

Values of constants in equation 2.2 are shown in Table 2.3.

Table 2.2: Co-efficient values for different spiral shapes.

Shape	c_1	c_2	c_3	c_4
Square	1.27	2.07	0.18	0.13
Hexagonal	1.09	2.23	0.00	0.17
Octagonal	1.07	2.29	0.00	0.19
Circle	1.00	2.46	0.00	0.20

Table 2.3: Monomial fit constants for different spiral shapes.

Shape	**β**	**$\alpha_1(d_{out})$**	**$\alpha_2(w)$**	**$\alpha_3(d_{avg})$**	**$\alpha_4(N)$**	**$\alpha_5(s)$**
Square	$1.62x\ 10^{-3}$	-1.21	-0.147	2.40	1.78	-0.030
Hexagonal	$1.28x\ 10^{-3}$	-1.24	-0.174	2.47	1.77	-0.049
Octagonal	$1.33x\ 10^{-3}$	-1.21	-0.163	2.43	1.75	-0.049

To find the shape with the highest inductance, we consider an inductor with the following specifications:

- No. of turns (N) = 4
- Spacing between turns (s) = 0.220 mm
- Turn width (w) = 0.5 mm
- Outer diam (d_{out}) = 10 mm
- Inner diameter (d_{in}) = 4.68 mm
- Fill factor (ρ) = 0.362

Using equations 2.1, 2.2, and 2.3, the inductance for four different shapes is calculated and displayed in Table 2.4. As evident from the values in Table 2.4, the square shape has the highest self-inductance for any given set of design and dimensional constraints. Therefore, we use the spiral inductor in a square spiral pattern for our study.

Table 2.4: Calculated inductance from different approximations

Shape	**Inductance (nH)**		
	Wheeler approximation (Equation 2.1)	**Current-Sheet approximation (Equation 2.2)**	**Monomial fit approximation (Equation 2.3)**
Square	172.963	171.014	178.579
Hexagonal	144.215	147.94	150.219
Octagonal	145.223	147.529	150.012
Circle	146.25	143.258	150.102

2.3 Design on FR-4 substrate

After selecting a square as the shape for our inductor design, we move towards the design of the inductor on FR-4. The main design constraint we set is the area. The square inductor's size is fixed at 1cm x 1cm. Other specifications are chosen as:

- No. of turns (N) = 6
- Turn width (w) = 500 µm
- Outer diameter (d_{out}) = 10 mm
- Inner diameter (d_{in}) = 1.8 mm
- Fill factor (ρ) = 0.695
- FR-4 substrate height = 1.4 mm
- Conductor thickness = 18 µm
- Spacing between turns (s) = 220 µm

Using the modified wheeler formula to calculate the inductance of this inductor using equation 2.1, we get an estimate of the total inductance to be equal to 214 nH. The inductor was then designed in CST Studio suite 2018 software. Ports are connected to the inductor such that it is divided into two sub-inductors. The first port is placed between the outermost turn and the fourth turn, making the first inductor; we call this as outer sub-inductor.

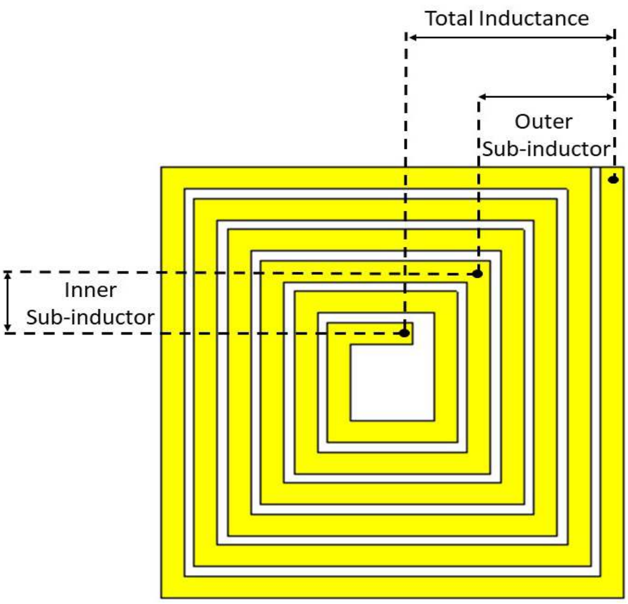

Figure 2.2: Design of proposed spiral inductor.

Tapping between the fourth and innermost turn makes the second inductor which we call the inner sub-inductor. The geometry of the design is shown in Figure 2.2.

2.4 Simulations

The inductor was designed in the CST microwave studio. A time domain simulation was performed. The time domain solver is based on the Finite Integration Technique (FIT) that uses a hexahedral mesh type. The first port is defined to calculate the total inductance between the outermost and innermost turn. A second port is defined between the outermost and fourth turn to calculate the inductance of the outer sub-inductor.

Figure 2.3 shows the second port's magnetic field lines and surface currents. The surface currents and the magnetic field strength is concentrated between the outermost and fourth turn. The third port is defined between the fourth and innermost turn for the inductance calculation of the inner sub-inductor. Figure 2.4 shows the third port's magnetic field lines and surface currents. It can be seen that the surface currents and most of the magnetic field strength are limited between the fourth and innermost turn.

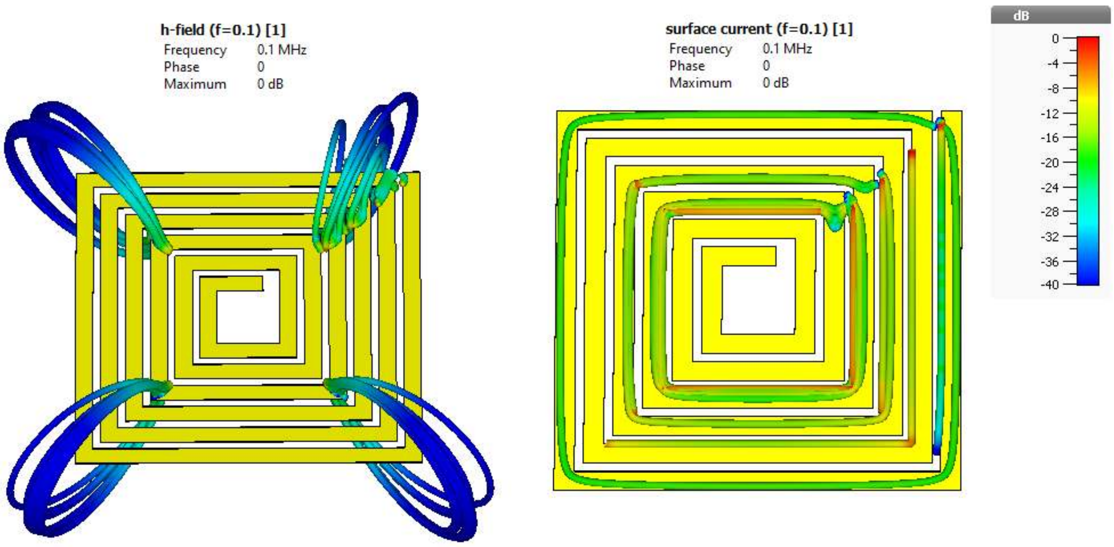

Figure 2.3: Simulated magnetic field and surface currents for the outer sub-inductor.

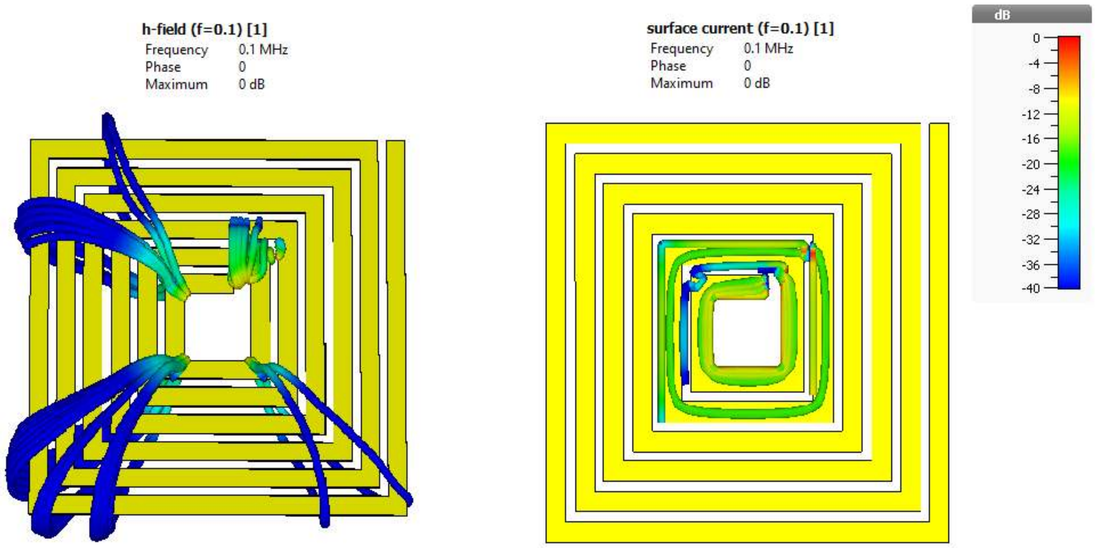

Figure 2.4: Simulated magnetic field and surface currents for the inner sub-inductor.

2.5 Fabrication and measurement

The inductor was fabricated on a double-sided FR-4 substrate. The fabrication was done using an LPKF protolaser U4. The inductor during fabrication is shown in Figure 2.5. At the three tapping points shown in Figure 2.2, via holes were made from top to bottom layer, where small pads were placed for measurement purposes. The inductance was then measured on Zurich instruments MFLIA impedance analyzer. A short-open-based calibration was performed to compensate for the effects of measurement cables. The simulated and measured inductance of the outer sub-inductor, inner sub-inductor, and total inductance are plotted in Figure 2.6.

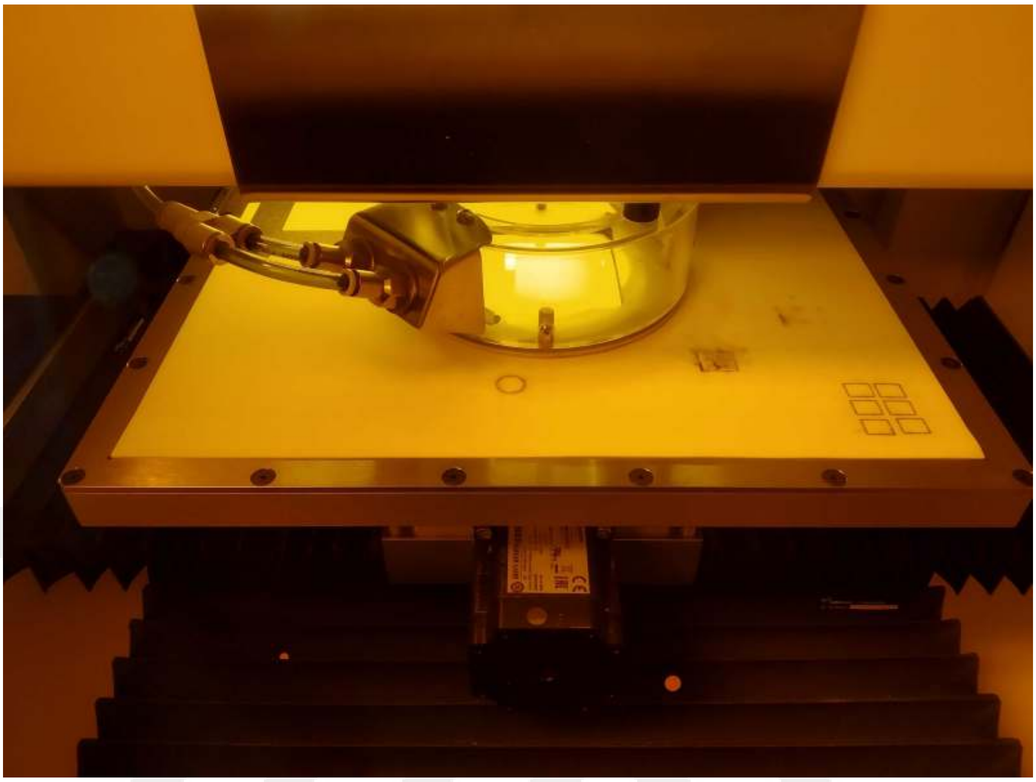

Figure 2.5: Fabrication on the LPKF protolaser U4.

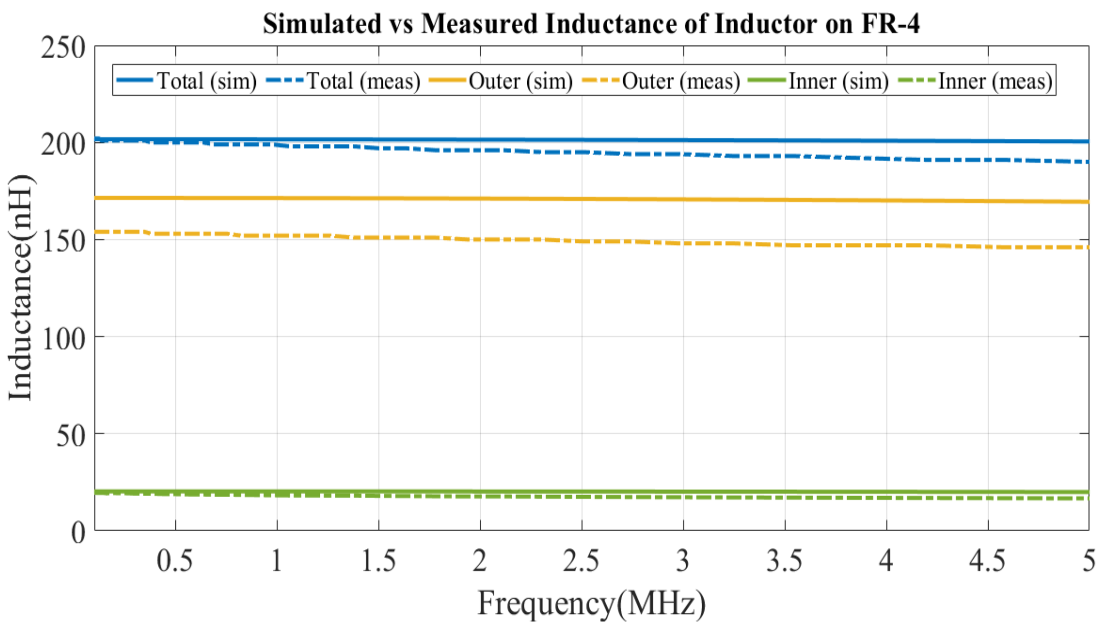

Figure 2.6: Simulated vs. measured inductance of the inductor and sub-inductors.

Chapter 3

INDUCTOR RESONANCE WITH VARIABLE CAPACITORS

3.1 Simulations

To verify the concept of dual resonance shift, simulations were first performed in CST microwave studio using a 3D-schematic co-simulation. To see the resonance shift, two LC circuits are made by connecting variable capacitors to each of the two sub-inductors. The layout is shown in Figure 3.1. A separate single loop inductor is used as the reader for resonance measurements. The port on which S11 is calculated is connected to the external loop. As explained in section 2.3, two other ports are connected to the inductor at the turns where the two sub-inductors are defined. The layout is first siaamulated using the time domain solver of CST microwave studio.

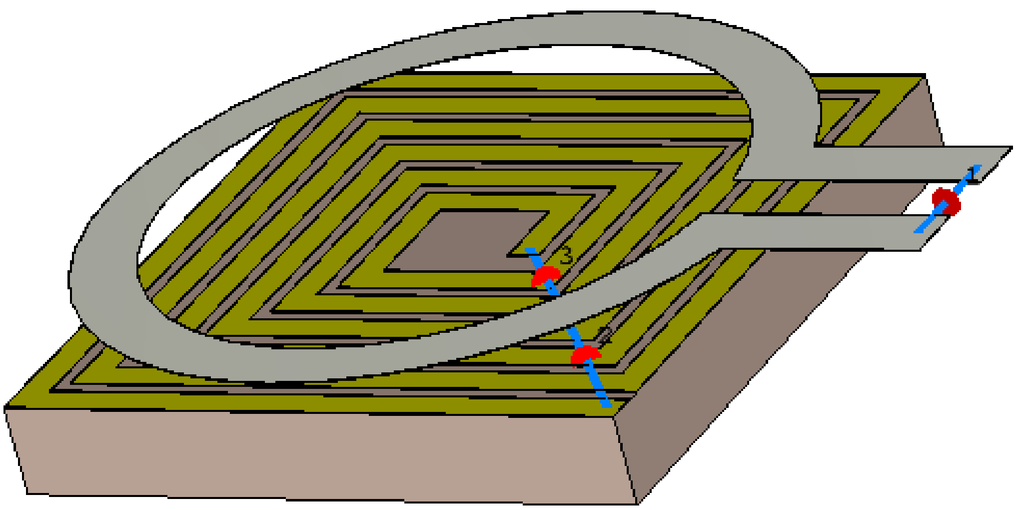

Figure 3.1: Layout of simulations for resonance frequency.

This model and its results are then exported to the schematic section of CST microwave studio. Two lumped capacitors are connected to the two sub-inductors. The capacitor C_1 is connected to the outer sub-inductor (outer coil) and C_2 to the inner sub-inductor (inner coil). The schematic layout is shown in Figure 3.2.

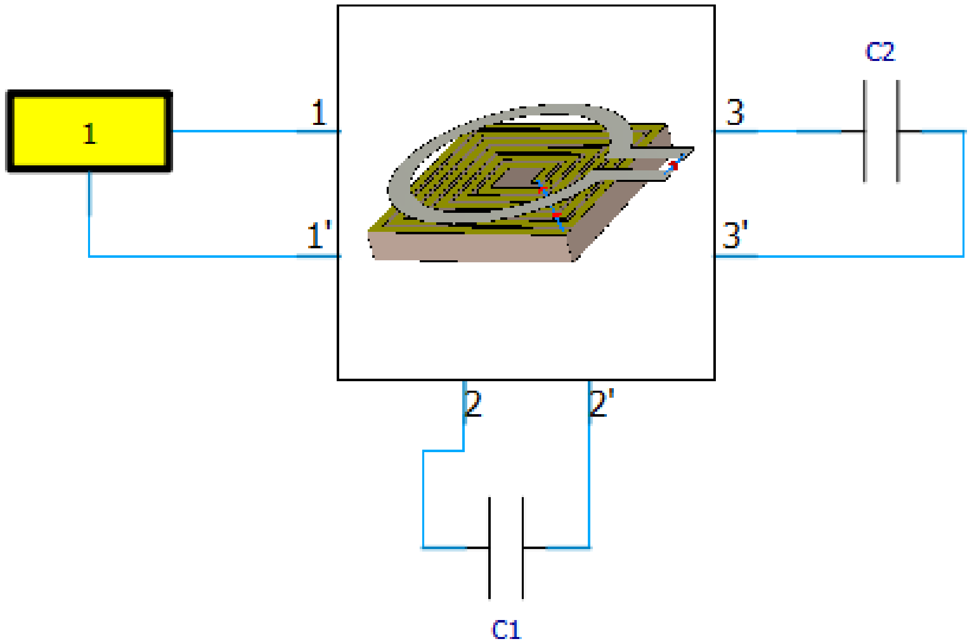

Figure 3.2: Schematic of co-simulation in CST Microwave Studio.

First, C_1 is varied while C_2 is kept constant. The LC circuit made by connecting the capacitor C_1 to the outer coil (L_1) leads to a lower resonance frequency (f_1) because of the higher value of L_1. The LC circuit with capacitor C_2 and inner coil (L_1) has a higher resonance frequency (f_2). The S11 vs. frequency is plotted for different values of C_1 in Figure 3.3. To match the simulations and experiments, the values of the capacitances used in the simulation correspond to the measured capacitances of the variable capacitors used in the subsequent experiments. Ideally, changing C_1 should only change the lower resonance frequency, but it can be seen that varying C_1 also changes the higher resonance frequency.

This effect is caused by mutual inductance between the two coils, as the magnetic field lines are not totally independent for both excitations and overlap. Decreasing C_1 increases the resonance frequency f_1 because they are inversely proportional, as formulated in equation 1.13. The S11 vs. frequency is plotted for different values of C_2 in Figure 3.4. It can be seen that varying C_2 changes only the higher resonance frequency, while the lower resonance remains constant.

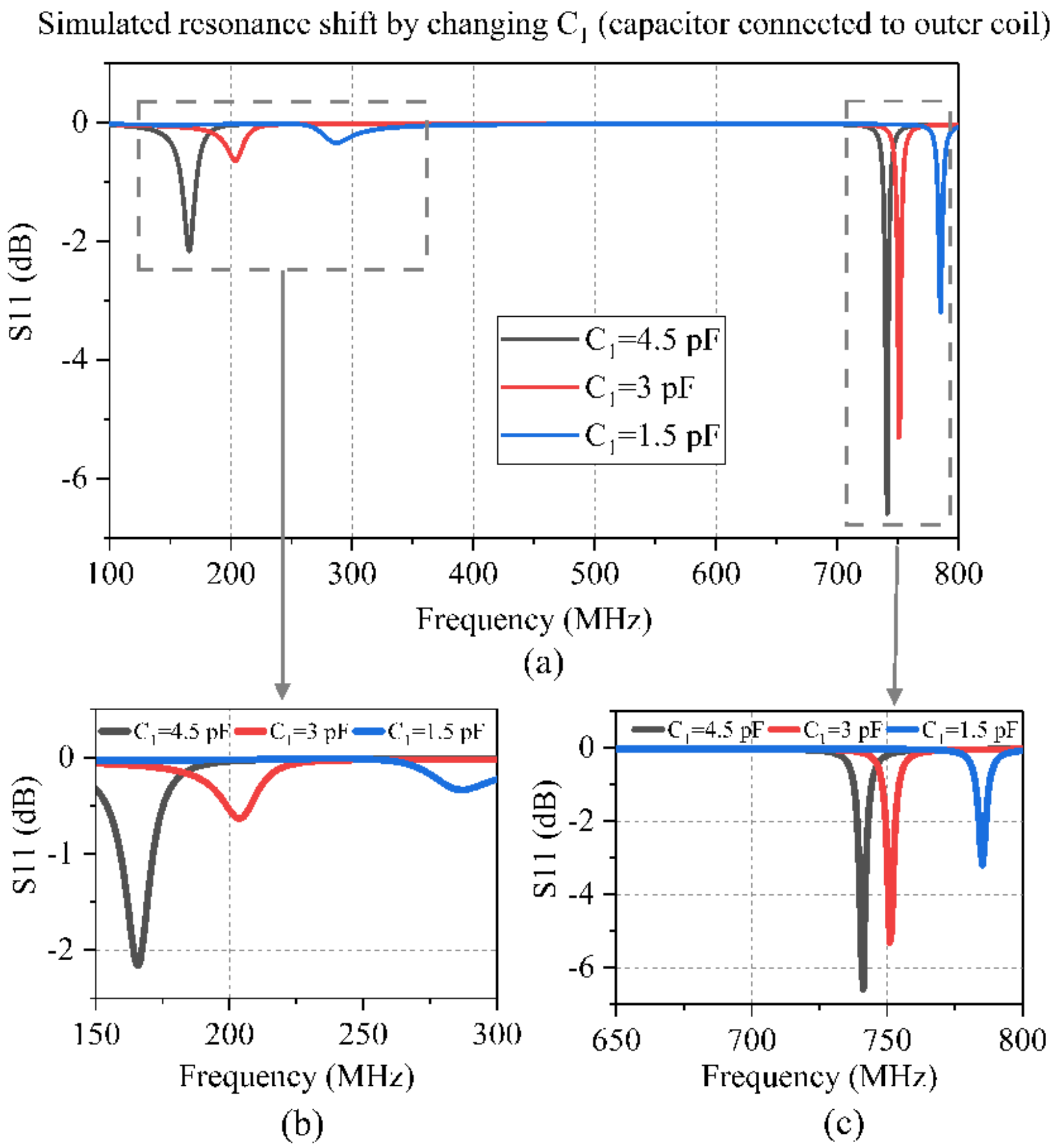

Figure 3.3: a) Simulated S11 vs. frequency plot by varying capacitor C_1 connected to outer coil. b) zoomed view around lower resonance frequency f_1. c) zoomed view around higher resonance frequency f_2.

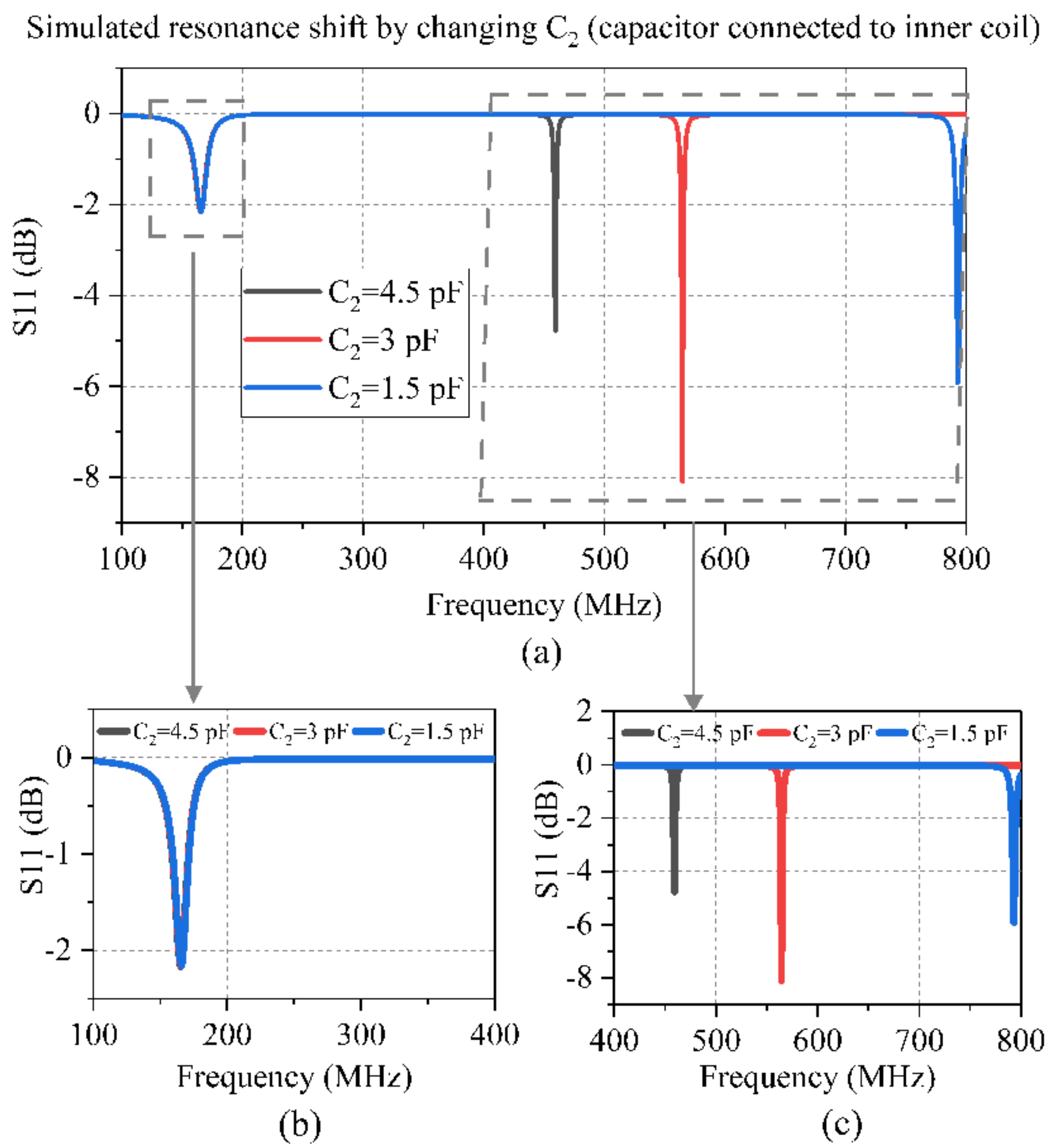

Figure 3.4: a) Simulated S11 vs. frequency plot by varying capacitor C_2 connected to inner coil. b) zoomed view around lower resonance frequency f_1. c) zoomed view around higher resonance frequency f_2.

3.2 Resonance frequency measurements

For measurements, two variable capacitors are attached to the two sub-inductors. Via holes are made, and connections are made by soldering pins of the variable capacitors to the back side of the inductor. The device is attached near another loop connected to a vector network analyzer (Siglent SVA 1032X).

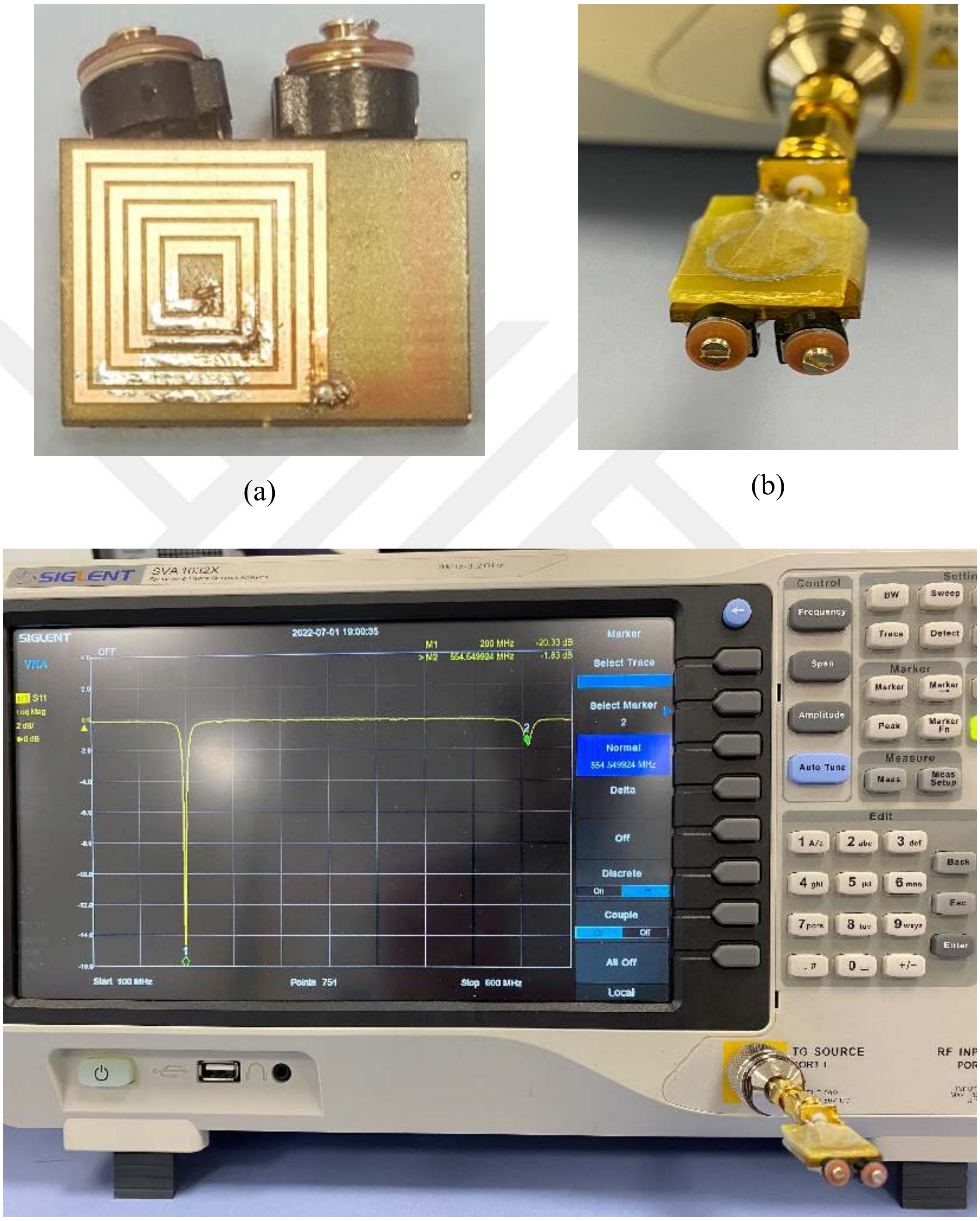

(a) (b)

(c)

Figure 3.5: a) Fabricated inductor with variable capacitors. b) fabricated device fixed near reader coil. c) S11 measurement on the vector network analyzer.

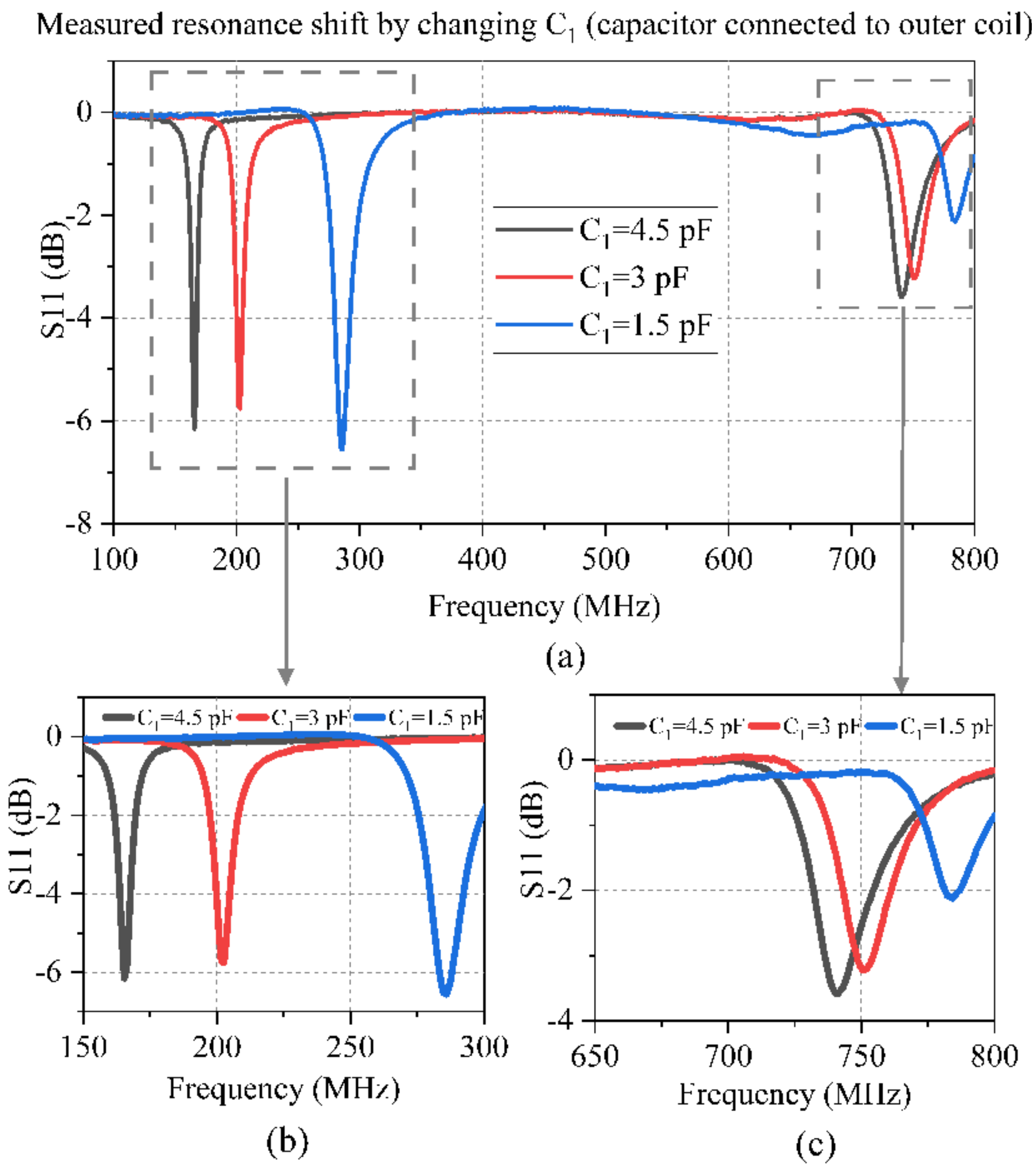

Figure 3.6: a) Measured S11 vs. frequency plot by varying capacitor C_1 connected to outer coil. b) zoomed view around lower resonance frequency f_1. c) zoomed view around higher resonance frequency f_2.

The fabricated device and measurement setup are shown in Figure 3.5. An S11 vs. frequency measurement is done while changing the variable capacitor connected to the external coil, i.e., C_1. The results are shown in Figure 3.6. The results are very close to simulations. Similar to simulations, both resonance frequencies change when C_1 is changed.

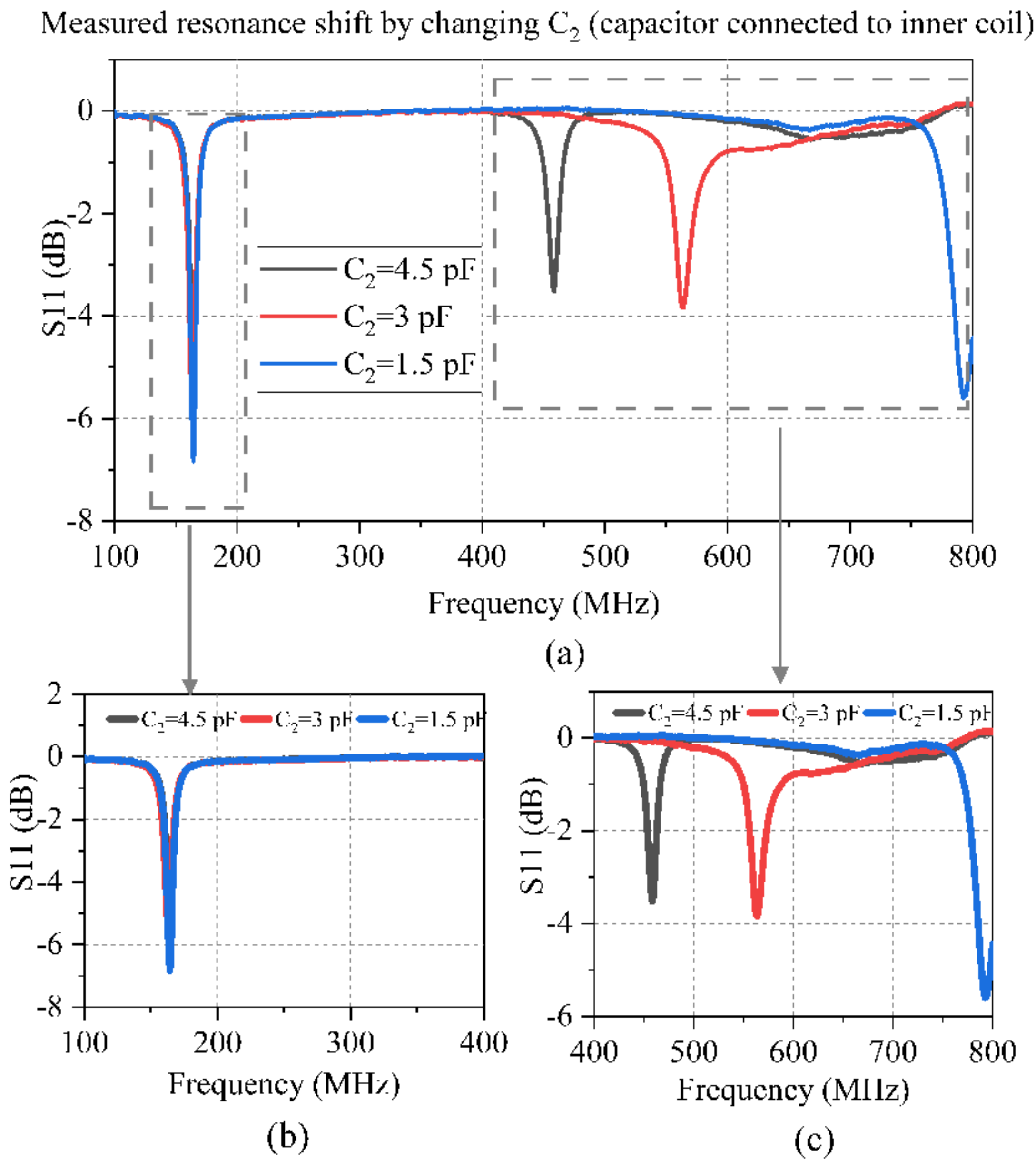

Figure 3.7: a) Measured S11 vs. frequency plot by varying capacitor C_2 connected to inner coil. b) zoomed view around lower resonance frequency f_1. c) zoomed view around higher resonance frequency f_2.

3.3 Simulations vs. measurements

The measurements and experiments for the case when C_1 is changed are compared in figure 3.8 for two values of C_1. The results show that the measured and simulated resonance frequencies match well.

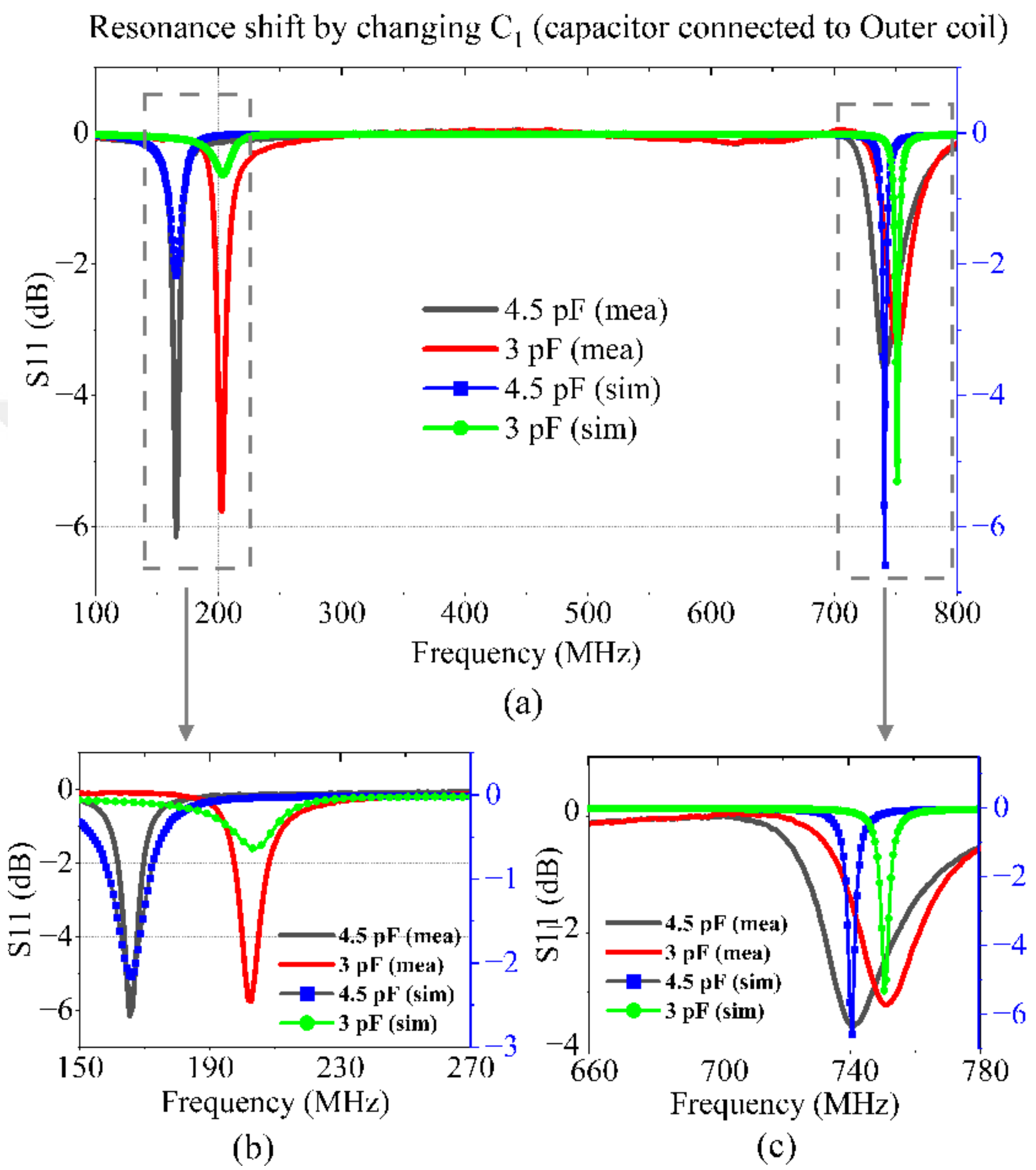

Figure 3.8: a) Measured vs. simulated S11 plot at two values of capacitor C_1 connected to outer coil. b) zoomed view around lower resonance frequency f_1. c) zoomed view around higher resonance frequency f_2.

The measurements and experiments for the case when C_2 is changed are compared in figure 3.9 for two values of C_2. The results show that the measured and simulated resonance frequencies match quite well.

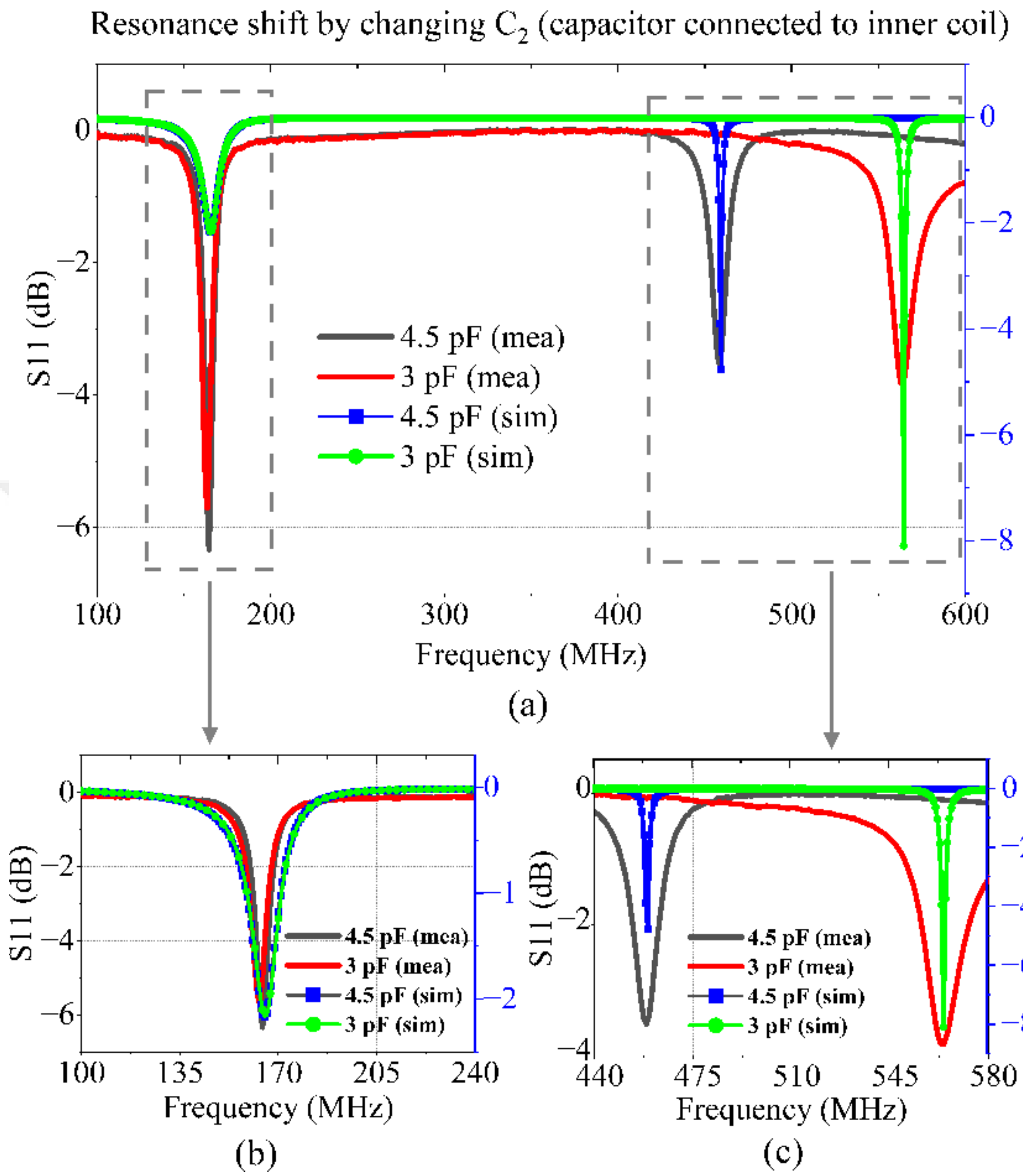

Figure 3.9: a) Measured vs. simulated S11 plot at two values of capacitor C_2 connected to the inner coil. b) zoomed view around lower resonance frequency f_1. c) zoomed view around higher resonance frequency f_2.

Due to the vias and tracks on the bottom side, the inductance values of the outer and inner coils are increased. The new inductance of the outer coil L_1= 205 nH and that of the inner coil L_2=26.6 nH. The theoretically calculated values of resonance frequencies for the case when C_1 is changed are compared with those from simulations and measurements in Table 3.1. The theoretically calculated values of resonance frequencies for the case when C_2 is changed are compared with those from simulations and measurements in Table 3.2.

Table 3.1: Calculated, simulated, and measured resonance frequencies vs. Capacitance C_1.

C_1 (pF)	$f_1=\frac{1}{2\pi\sqrt{L_1C_1}}$ (MHz)	f_1 Simulated (MHz)	f_1 Measured (MHz)
4.5	165.70	165.87	165.33
3.0	202.94	203.7	202.67
1.5	287.01	287.09	285.73

Table 3.2: Calculated, simulated, and measured resonance frequencies vs. Capacitance C_2,

C_2 (pF)	$f_2=\frac{1}{2\pi\sqrt{L_2C_2}}$ (MHz)	f_2 Simulated (MHz)	f_2 Measured (MHz)
4.5	460.88	459.46	458.4
3.0	564.46	546.56	563.86
1.5	798.27	792.99	792.53

Chapter 4

MULTI-RESONANCE INDUCTOR WITH STRAIN SENSORS

To check the practicality of the device, the inductor was coupled with two strain sensors. The strain sensors are basically interdigitated capacitors fabricated on a flexible substrate (PDMS). The electrode gaps of the two strain sensors are 0.1mm and 0.05 mm, respectively. The 0.05mm gap strain sensor is attached to the outer sub-inductor and the 0.1mm gap strain sensor to the inner sub-inductor.

4.1 Interdigitated capacitive strain sensors (ICSSs)

Typically, a capacitor consists of a dielectric layer sandwiched between two electrodes. The capacitance is generally defined as $C=\epsilon_0\epsilon_r A/d$, where ϵ_0 is the permittivity of vacuum, ϵ_r is the dielectric's relative permittivity, A is the area of electrodes, and d is the separation between electrodes. An ICSS has two interlocked comb-shaped arrays of metallic electrodes [Zhang *et al.*, 2022]. When the capacitor is stretched in-plane in the direction perpendicular to the electrodes, it increases the distance (*d*) between any two electrodes while the thickness and length of the electrodes decrease, leading to a decrease in the area (*A*). Therefore, decreasing *A* and increasing *d* leads to a reduction of the capacitance of the ICSS [Jia *et al.*, 2006] [Zhang *et al.*, 2022]. In this study, two ICSSs with different initial electrode gaps (0.05mm and 0.1mm) are fabricated on a flexible substrate (PDMS) to be used as strain sensors. From here on, the sensor with an electrode gap of 0.05 mm will be called sensor 1, and the one with a 0.1mm electrode gap will be called sensor 2. The fabricated strain sensors are shown in Figure 4.1.

4.1 Simulations

CST microwave studio was used to carry out the simulations. The strain sensors were attached with the inductor using jumper wires. For flexibility, PDMS is used as the substrate. However, the strain sensors need to be placed on the translational stage device for measurement purposes. Therefore, the wires between strain sensors and the inductor must be extended.

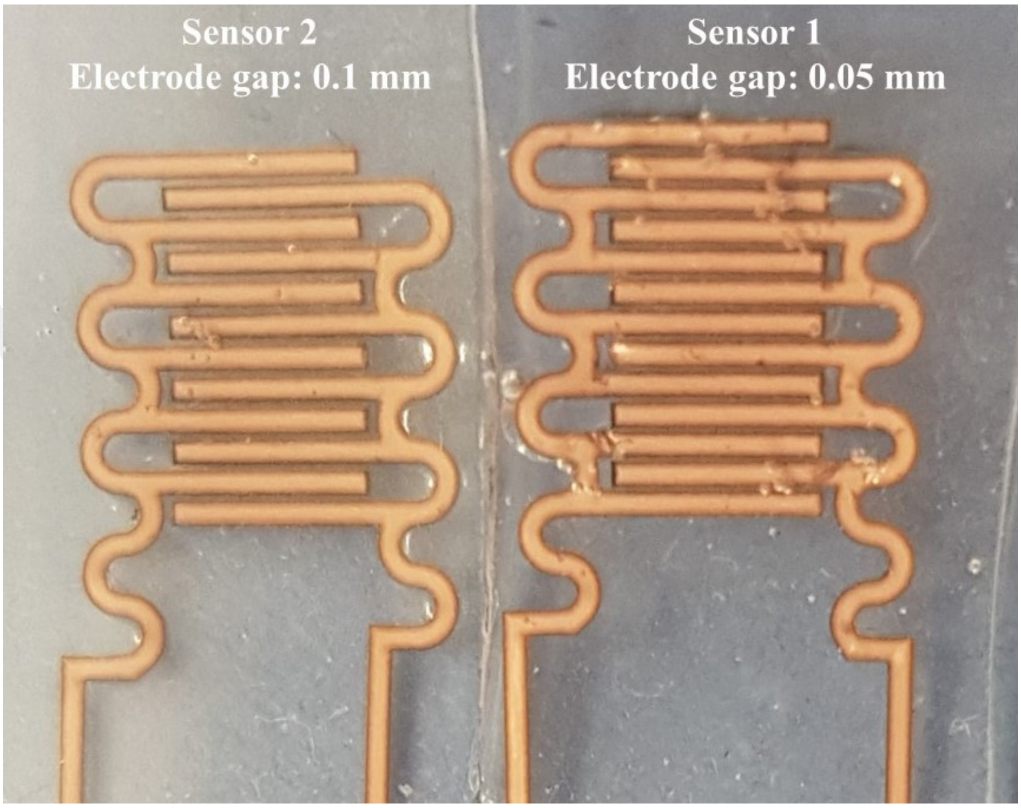

Figure 4.1: Fabricated strain sensors.

These wires are added in the simulations too. A port is attached to a reader loop, and S11 is simulated against frequency. A screenshot of the simulation is shown in Figure 4.2. The S11 vs. frequency plot is shown in Figure 4.3. Two resonance frequencies occur. The lower resonance frequency (f_1) is due to the LC circuit composed of the outer coil and sensor 1 (electrode gap of 0.05 mm). The higher resonance frequency results from the LC circuit made by the inner coil and sensor 2 (electrode gap of 0.1 mm).

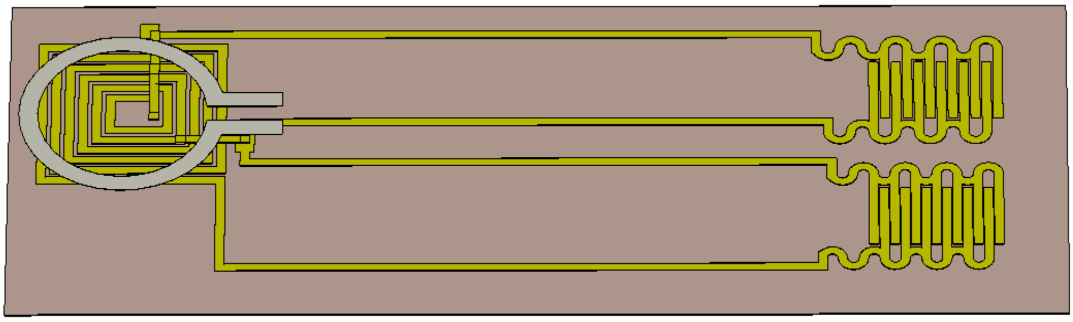

Figure 4.2: Simulation layout of inductor and strain sensors with reader coil.

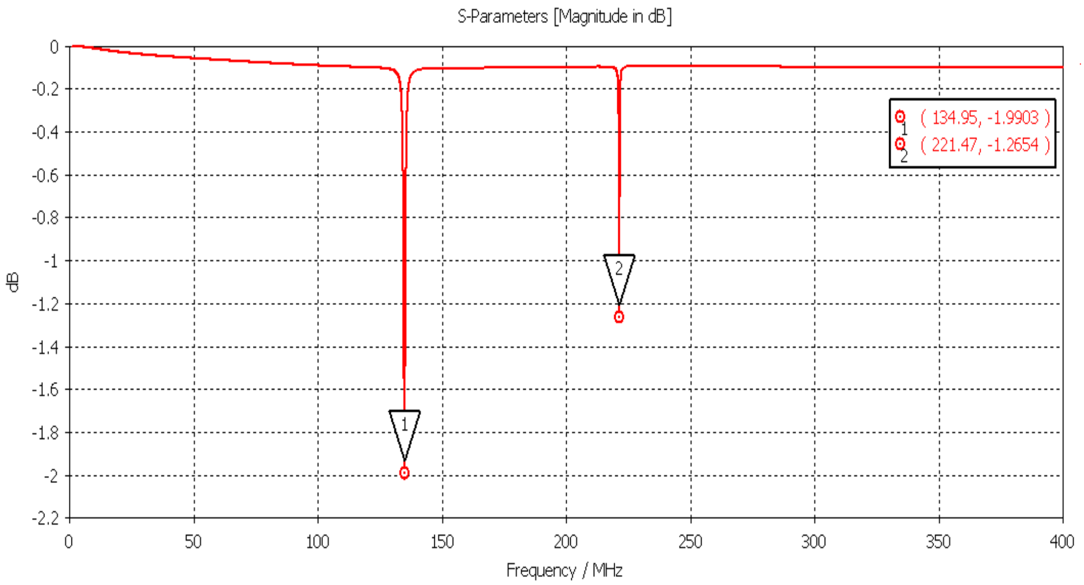

Figure 4.3: Simulated S11 for the circuit of Figure 4.2.

4.2 Capacitance measurement of strain sensors

The capacitance of the two strain sensors is first measured using an impedance analyzer (Zurich Instruments MFLIA). The strain sensors are placed on a motorized translation stage (Thor labs MTS50/M-Z8), stretching them. Different strain levels are applied, and capacitance is measured. Figure 4.4a plots the capacitance vs. strain for sensor 1, and the same is plotted in Figure 4.4b for strain sensor 2. As the sensor 1 has a lower electrode gap of 0.05 mm, it should have higher capacitance than sensor 2, which has an electrode gap of 0.1mm. This inverse relationship between electrode gap and capacitance is verified by Figure 4.4c, which shows that the capacitance of sensor 1 is higher than that of sensor 2. Additionally, when strain increases, the electrode gaps increase further, which leads to a decrease in capacitance, verified by Figure 4.4.

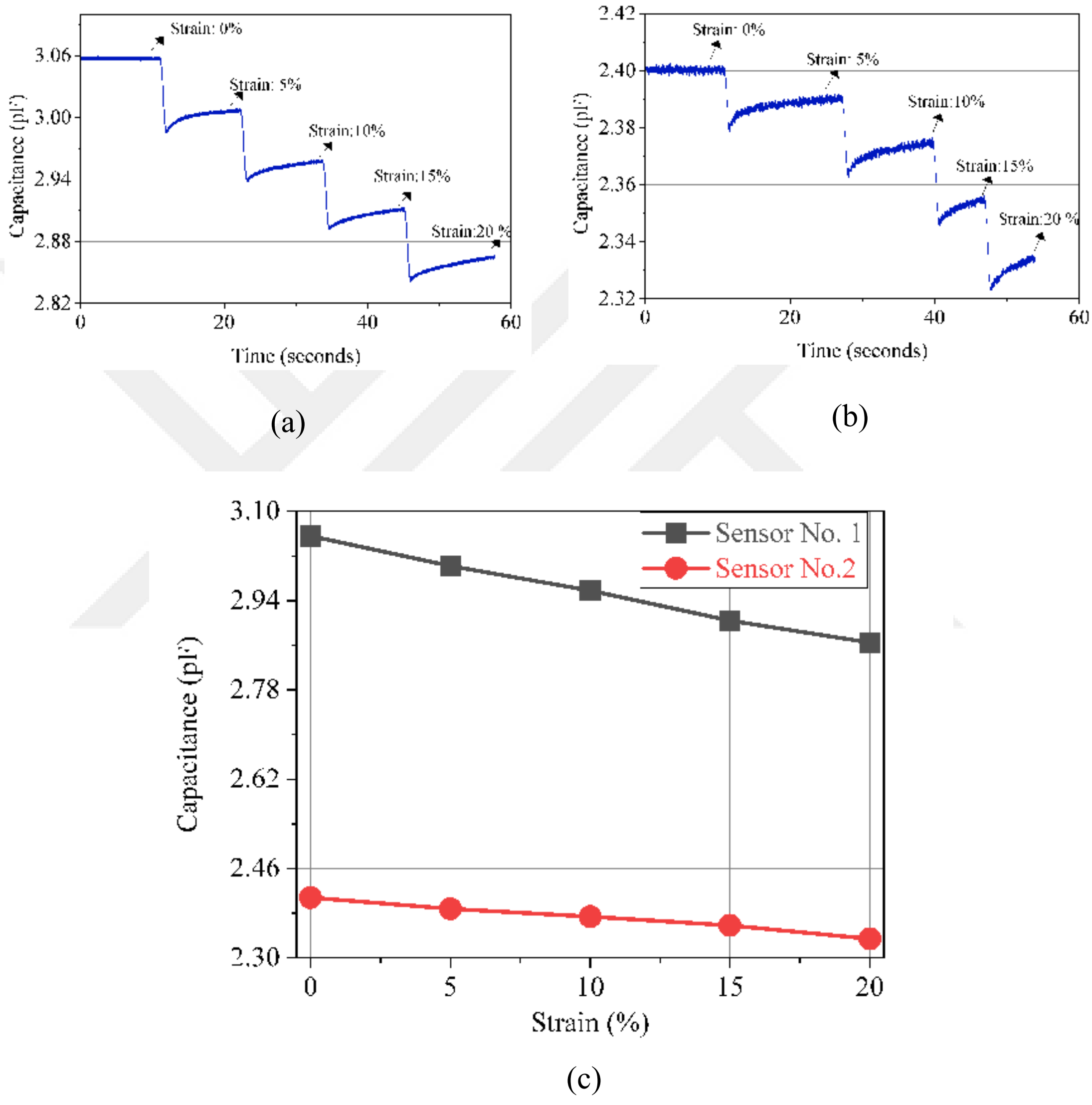

(a) (b) (c)

Figure 4.4: a) Capacitance of sensor 1 as different strain is applied vs. time. b) capacitance of sensor 2 as different strain is applied vs. time. c) capacitance of both strain sensors vs. strain.

4.3 Resonance frequency vs. strain measurement for sensor 1

The resonance measurement setup is shown in Figure 4.5, where the strain sensors are connected to the inductor through wires. The inductor is placed close to the reader loop antenna, which is connected to the vector network analyzer. First, sensor 1 is fixed on the strain gauge, and strain is applied while no strain is applied to sensor 2. The S11 vs. frequency measurement results are shown in Figure 4.6.

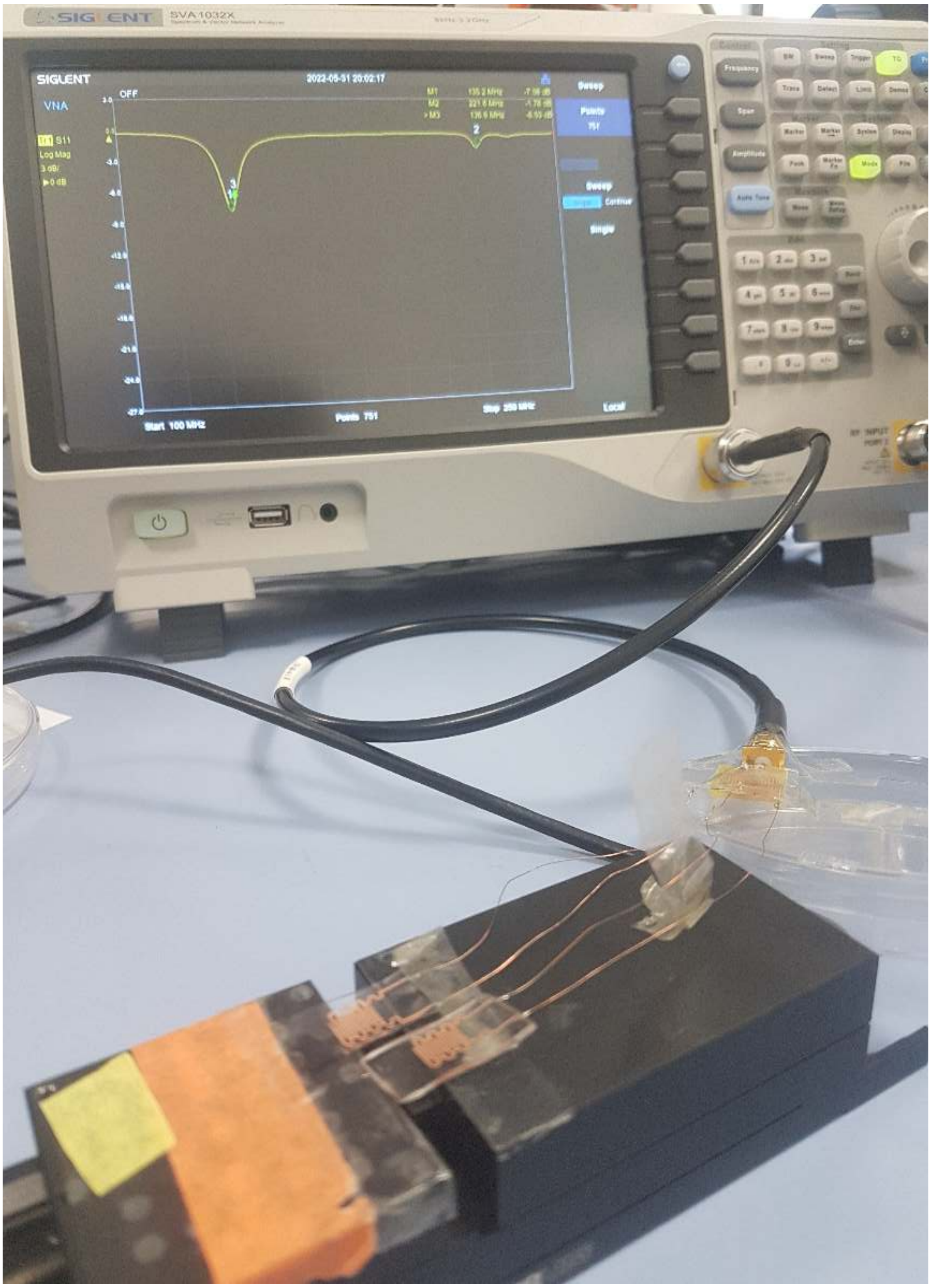

Figure 4.5: Experimental setup for resonance frequency vs. strain measurements.

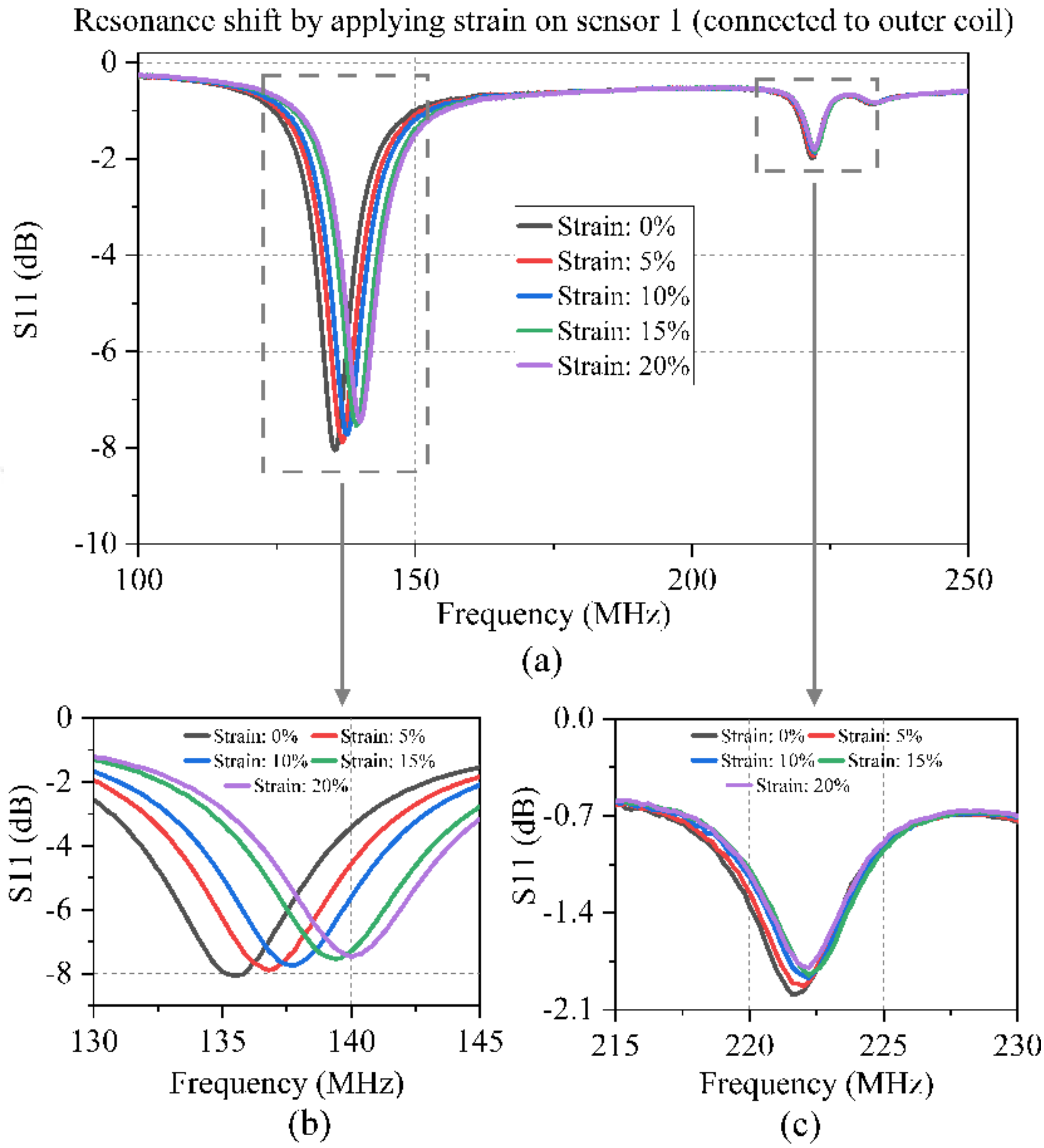

Figure 4.6: a) Measured S11 vs. frequency plot as strain is applied on sensor 1. b) zoomed view around lower resonance frequency f_1. c) zoomed view around higher resonance frequency f_2.

Similar to the measurements with the variable capacitors in section 3.2, increasing strain on sensor 1 changes both the resonance frequencies. The increased strain causes a decrease in capacitance, leading to the increased resonance frequency. The lower and higher resonance frequencies f_1 and f_2 are tabulated in Table 4.1.

Table 4.1: Resonance frequencies vs. strain on sensor 1.

Strain (%)	**f_1 (MHz)**	**f_2 (MHz)**
0	135.6	222.0
5	136.8	222.2
10	137.8	222.4
15	139.2	222.6
20	140	222.6

4.4 Resonance frequency vs. strain measurement for sensor 2

After sensor 1 measurements, sensor 2 is fixed on the strain gauge, and strain is applied on this sensor while no strain is applied to sensor 1. The S11 vs. frequency measurement results are shown in Figure 4.7. The increased strain caused a decrease in capacitance, leading to the increased resonance frequency. It can be noted that only the higher resonance frequency shifts, and the lower one remains constant. The lower (f_1) and higher (f_2) resonance frequencies against strain on sensor 2 are shown in Table 4.2.

Table 4.2: Resonance frequencies vs. strain on sensor 2

Strain (%)	**f_1 (MHz)**	**f_2 (MHz)**
0	135.6	222.0
5	135.6	223.2
10	135.6	223.8
15	135.6	224.4
20	135.6	225.8

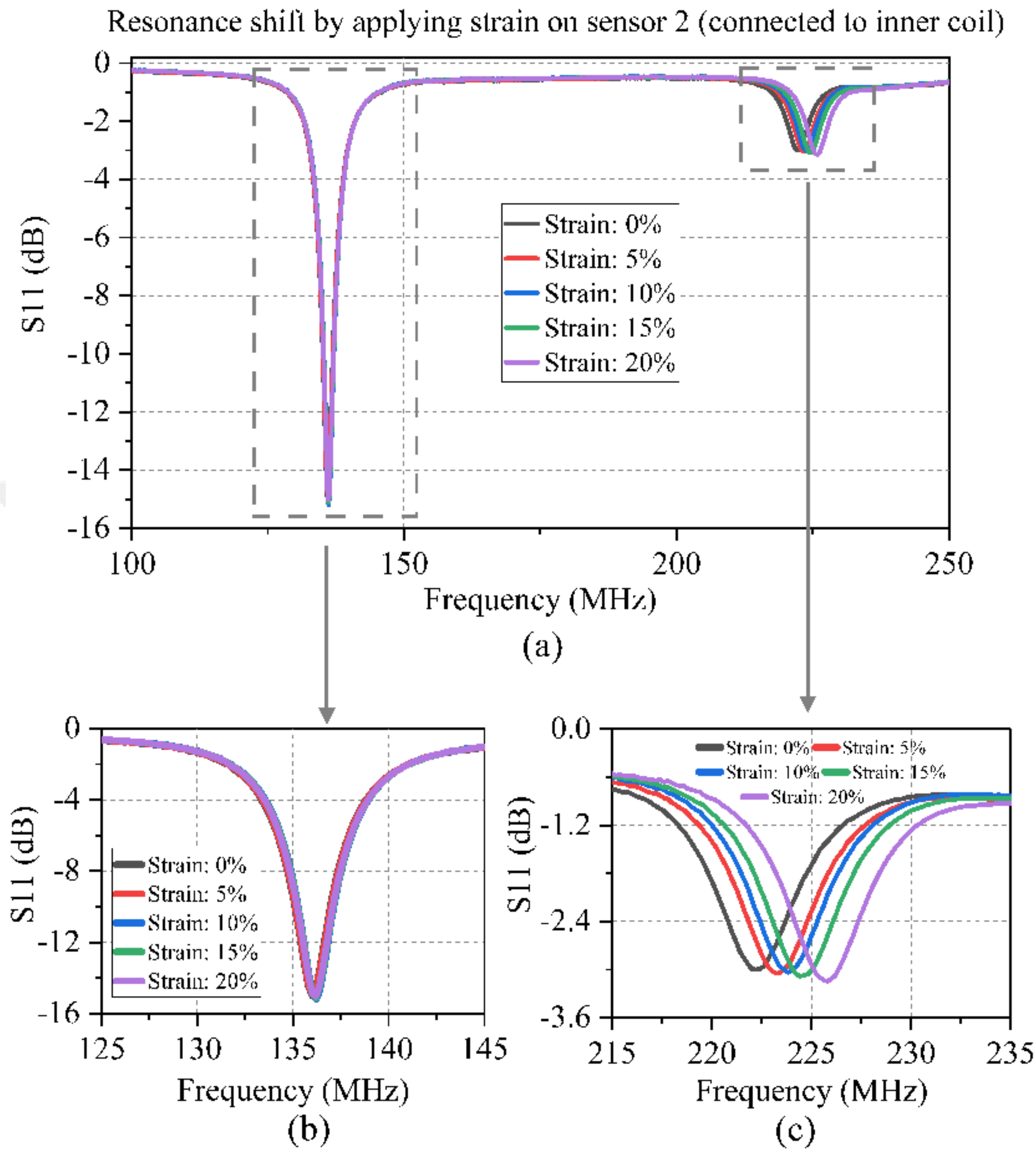

Figure 4.7: a) Measured S11 vs. frequency plot as strain is applied on sensor 2. b) zoomed view around lower resonance frequency f_1. c) zoomed view around higher resonance frequency f_2.

4.5 Strain value extraction from resonance frequencies

To extract the strain values of the sensors from resonance frequencies, linear curve fitting is done. First, the lower (f_1) and higher (f_2) resonance frequencies are plotted against strain in Figures 4.8a and 4.8b, respectively, for the case when strain is applied on sensor 1. The fitted curves are also plotted in the same figures. The fitted curve for both resonance frequencies against strain on sensor 1 are:

$$f_1=135.64+0.224s_1 \quad (4.1)$$

$$f_2'=222.04+0.032s_1 \quad (4.2)$$

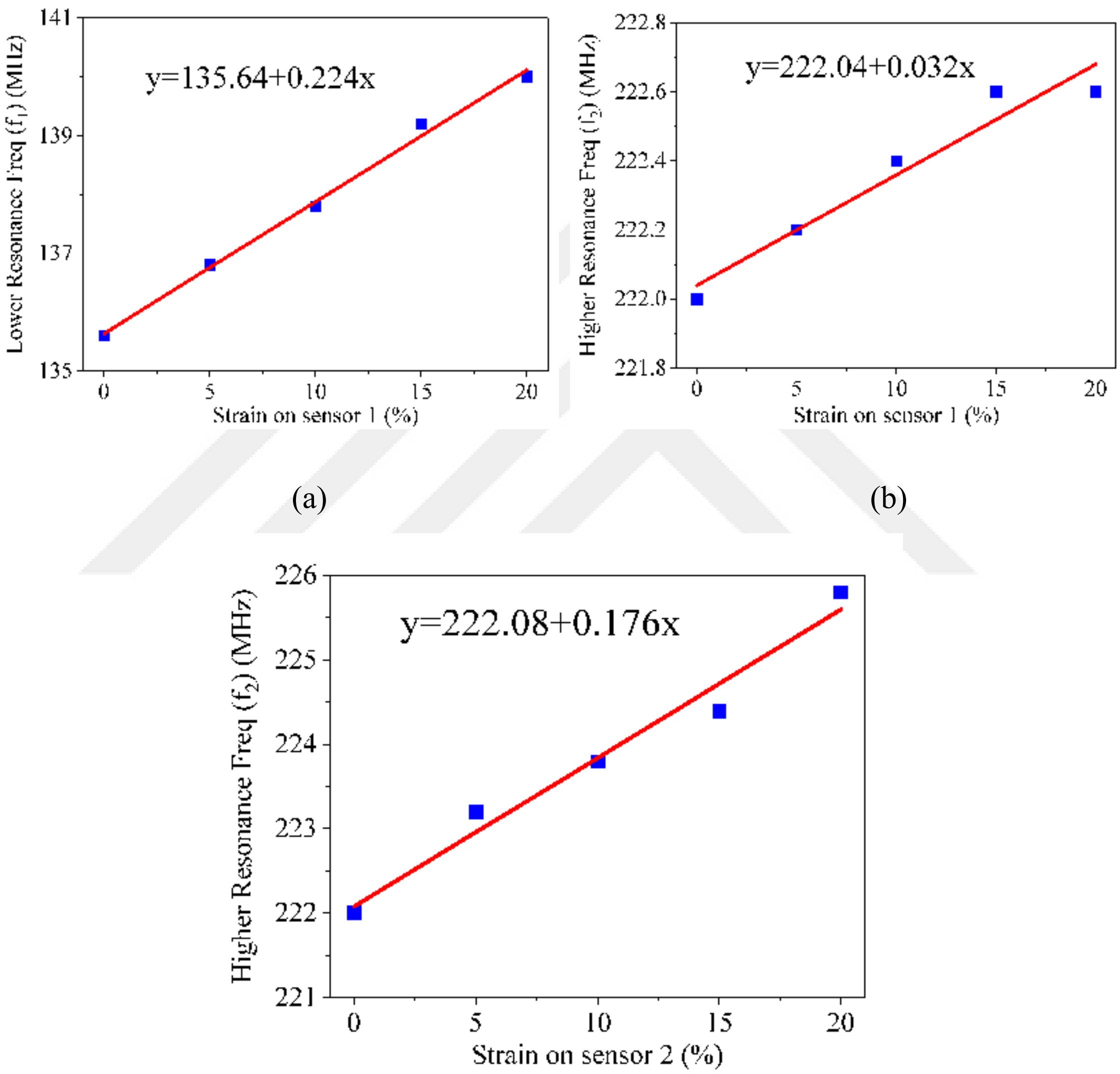

(a) (b) (c)

Figure 4.8: a) Fitted resonance frequency curve for lower resonance frequency (f_1) vs. strain applied on sensor 1. b) Fitted resonance frequency curve for higher resonance frequency (f_2) vs. strain applied on sensor 1. c) Fitted resonance frequency curve for higher resonance frequency (f_2) vs. strain applied on sensor 2.

Here, the frequencies are in MHz, and the strain value s_1 is percent strain on sensor 1. When strain is applied on sensor 2, only the higher resonance frequency (f_2) changes. f_2 is plotted against the strain on sensor 2, along with the fitted curve in Figure 4.8c. The fitted curve for f_2 is:

$$f_2=222.08+0.176s_2 \quad (4.3)$$

Where s_2 is the percent strain on sensor 2. The methodology for retrieving strain values of both sensors is as follows:

1. To get the strain percent value on sensor 1, note the lower resonance frequency f_1 and put it in equation 4.1 to get the value of strain s_1 on sensor 1.
2. To get strain percent value on sensor 2, there are three steps.
   a. Put the value of s_1 from step 1 in equation 4.2 to get the value of f_2'. This is the shifted higher resonance frequency because of sensor 1. This shift will be removed in the next step.
   b. In case when there is no strain on sensor 2, f_2 should be equal to the y-intercept of equation 4.3, i.e., 222.08. Therefore, the shift due to sensor 1 is calculated by finding the difference between f_2' and y-intercept. Let's call this shift c:

$$c=f_2'-222.08 \quad (4.4)$$

   c. The actual f_2 value is then found by subtracting this shift from the noted higher resonance frequency:

$$f_2=\text{Higher resonance frequency}-c \quad (4.5)$$

   d. Now use this value in equation 4.3 to get strain percent value s_2.

The procedure can be better understood by an example. Suppose we make an S11 measurement with the following resonance frequencies.

- Lower resonance frequency (f_1): 137.8 MHz
- Higher resonance frequency: 223.4 MHz

1. Putting value of f_1 in equation 4.1, we get $s_1 = 9.64 \sim 10$
2. Using s_1=10,
   a. Putting value of s_1 in equation 4.2, we get f_2'= 222.36
   b. From equation 4.4, c=222.36-222.08=0.28
   c. Put value of c in equation 4.5, f_2=223.4-0.28=232.12
   d. Putting f_2 value in equation 4.3, we get s_2=5.9~5

Therefore, we get the strain value of sensor 1 as 10% and the strain value of sensor 2 as 5%.

Chapter 5

CONCLUSION

LC based passive wireless sensors are frequently deployed for sensing in harsh environments and implant applications. The demand for sensing multiple parameters is ever-increasing. At the same time, the sensor size needs to be as low as possible. In this work, one inductor is connected to two sensors at different turns rather than just the inner and outermost turns. This way, the inductor is divided into two inductors, each connected to a capacitive sensor to make two LC circuits. When placed near an external reader coil, the system shows two resonance frequencies, one for each of the two LC circuits.

The lower resonance frequency is related to the outer coil and sensor connected to it, and the higher resonance frequency is associated with the inner coil and its sensor. The value of the sensor connected to the outer coil can be estimated from the lower resonance frequency. The higher resonance frequency is dependent on both the sensors connected to inner, as well as outer coil. To evaluate the sensor's value connected to the inner coil, the effect of the outer coil on the higher resonance frequency must be removed. For this purpose, calibration curves relate the strain value to the resonance frequencies. Using these, the effect of the outer coil on higher resonance is also removed, and we get the value of the sensor connected to the inner coil.

This work proposes a solution to multiple parameter sensing using a single inductor. Future work can be done to minimize the coupling between the sub-inductors to make the two LC circuits as independent as possible. The effect of tissue between the reader and sensor coils on the range and coupling can also be investigated.

BIBLIOGRAPHY

[Akhtar, 2021] Akhtar, M.J., 2021. Simulation of bulk piezoelectric implant with amplitude modulation-based backscatter communication for implant applications, pp. 2021–2023.

[Alexander *et al.*, 2006] Alexander, C., Alexander, C.K. and Sadiku, M.N.O., 2006. McGraw-Hill Higher Education. *Fundamentals of Electric Circuits*.

[Babu and George, 2016] Babu, A. and George, B., 2016. A linear and high sensitive interfacing scheme for wireless passive LC sensors, *IEEE Sensors Journal*, 16(23), pp. 8608–8616.

[Barakat *et al.*, 2019] Barakat, A., Yoshitomi, K. and Pokharel, R.K., 2019. Design and implementation of dual-mode inductors for dual-band wireless power transfer systems, *IEEE Transactions on Circuits and Systems II: Express Briefs*, 66(8), pp. 1287–1291.

[Bhadra *et al.*, 2013] Bhadra, S., Tan, D.S.Y., Thomson, D.J., Freund, M.S. and Bridges, G.E., 2013. A wireless passive sensor for temperature compensated remote pH monitoring, *IEEE Sensors Journal*, 13(6), pp. 2428–2436.

[Bhar and Mandal, 2022] Bhar, I. and Mandal, N., 2022. A review on advanced wireless passive temperature sensors, *Measurement: Journal of the International Measurement Confederation*, 187(July 2021), p. 110255.

[Bolz, 1970] Bolz, R.E., 1970. CRC Press. Electrical Science and Radiation, in *CRC Handbook of tables for Applied Engineering Science*. 2nd edn.

[Degen, 2021] Degen, C., 2021. Inductive coupling for wireless power transfer and near - field communication, *EURASIP Journal on Wireless Communications and Networking* [Preprint].

[Deng *et al.*, 2019] Deng, W.J., Zhou, B. Bin, Xie, M.Z., Wang, L.F., Dong, L., Huang, Q.A. and Yi, Z.X., 2019. Implementation of Four-parameter LC Sensing Through Symmetric Dual-Resonant Circuit, *Proceedings of IEEE Sensors*, 2019-Octob(2018), pp. 2019–2022.

[Dong *et al.*, 2019] Dong, L., Deng, W.J., Wang, L.F. and Huang, Q.A., 2019. Multi-Parameters Detection Implemented by LC Sensors with Branching Inductors, *IEEE Sensors Journal*, 19(1), pp. 304–310.

[Dong *et al.*, 2015] Dong, L., Wang, L.F. and Huang, Q.A., 2015. Implementation of multi-parameter monitoring by an LC-type passive wireless sensor through specific-winding, stacked inductors, *IEEE Internet of Things Journal*, 2(2), pp. 168–174.

[Dong *et al.*, 2016] Dong, L., Wang, L.F. and Huang, Q.A., 2016. An LC passive wireless multifunctional sensor using a relay switch, *IEEE Sensors Journal*, 16(12), pp. 4968–4973.

[Huang *et al.*, 2016] Huang, Q.A., Dong, L. and Wang, L.F., 2016. LC Passive Wireless Sensors Toward a Wireless Sensing Platform: Status, Prospects, and Challenges, *Journal of Microelectromechanical Systems*, 25(5), pp. 822–841.

[Jia *et al.*, 2006] Jia, Y., Sun, K., Agosto, F.J. and Quiñones, M.T., 2006. Design and characterization of a passive wireless strain sensor, *Measurement Science and Technology*, 17(11), pp. 2869–2876.

[Karimi *et al.*, 2021] Karimi, M.J., Schmid, A. and Dehollain, C., 2021. Wireless Power and Data Transmission for Implanted Devices via Inductive Links: A Systematic Review, *IEEE Sensors Journal*, 21(6), pp. 7145–7161.

[Li *et al.*, 2015] Li, C., Tan, Q., Jia, P., Zhang, W., Liu, J., Xue, C. and Xiong, J., 2015. Review of Research Status and Development Trends of Wireless Passive LC Resonant Sensors for Harsh Environments, *Sensors*, 15(6), pp. 13097–13109.

[Lin *et al.*, 2021] Lin, B., Tan, Q., Member, S., Zhang, G., Zhang, L., Wang, Y. and Xiong, J., 2021. Temperature and Pressure Composite Measurement System Based on Wireless Passive LC Sensor, 70.

[Luo and Wei, 2018] Luo, Z. and Wei, X., 2018. Analysis of Square and Circular Planar

Spiral Coils in Wireless Power Transfer System for Electric Vehicles, *IEEE Transactions on Industrial Electronics*, 65(1), pp. 331–341.

[Mohan *et al.*, 1999] Mohan, S.S., Hershenson, M.D.M., Boyd, S.P. and Lee, T.H., 1999. Simple accurate expressions for planar spiral inductances, *IEEE Journal of Solid-State Circuits*, 34(10), pp. 1419–1420.

[Dey et al., 2019] Nilanjan Dey;Amira S. Ashour;Simon James Fong;Chintan Bhatt, 2019. Elsevier Inc. *Wearable and Implantable Medical Devices: Applications and Challenges*. 1st edn, *Academic Press*. 1st edn.

[Nopper *et al.*, 2010] Nopper, R., Niekrawietz, R. and Reindl, L., 2010. Wireless readout of passive LC sensors, *IEEE Transactions on Instrumentation and Measurement*, 59(9), pp. 2450–2457.

[Sancho *et al.*, 2019] Sancho, J.I., Perez, N., De Nó, J. and Mendizabal, J., 2019. Implementation of simultaneous multi-parameter monitoring based in LC-type passive wireless sensing with partial overlapping and decoupling coils, *Sensors (Switzerland)*, 19(23).

[Stojanovic and Zivanov, 2004] Stojanovic, G. and Zivanov, L., 2004. Comparison of optimal design of different spiral inductors, in *2004 24th International Conference on Microelectronics (IEEE Cat. No.04TH8716)*, pp. 613–616 vol.2.

[Wheeler, 1928] Wheeler, H.A., 1928. Simple inductance formulas for radio coils, *Proceedings of the Institute of Radio Engineers*, 16(10), pp. 1398–1400.

[Zhang *et al.*, 2022] Zhang, D., Zhang, J., Wu, Y., Xiong, X., Yang, J. and Dickey, M.D., 2022. Liquid Metal Interdigitated Capacitive Strain Sensor with Normal Stress Insensitivity, *Advanced Intelligent Systems*, 4(4), p. 2100201.

[Zhang *et al.*, 2019] Zhang, G., Tan, Q., Lin, B. and Xiong, J., 2019. A Novel Temperature and Pressure Measuring Scheme Based on LC Sensor for Ultra-High Temperature Environment, *IEEE Access*, 7, pp. 162747–162755.

[Zhang *et al.*, 2012] Zhang, S., Pasupathy, P. and Neikirk, D.P., 2012. Microfabricated selfresonant structure as a passive wireless dielectric constant and conductivity sensor, *Microsystem Technologies*, 18(7–8), pp. 885–891.

[Zhou *et al.*, 2021] Zhou, Y., Dong, L., Zhang, C., Wang, L. and Huang, Q., 2021. Rotational Speed Measurement Based on LC Wireless Sensors, *Sensors*, 21(23).